Department of Neuroscience and Biomedical Engineering

The cardiomagnetic field: Non-invasive mapping of atrial fibrillation and model-based characterization of sensitivity and resolution

Ville Mäntynen

Aalto University

DOCTORAL DISSERTATIONS

Aalto University publication series
DOCTORAL DISSERTATIONS 106/2017

The cardiomagnetic field: Non-invasive mapping of atrial fibrillation and model-based characterization of sensitivity and resolution

Ville Mäntynen

A doctoral dissertation completed for the degree of Doctor of Science (Technology) to be defended, with the permission of the Aalto University School of Science, at a public examination held in Auditorium F239 at the Aalto University School of Science (Espoo, Finland) on 20 October 2017 at 12 noon.

Aalto University
School of Science
Department of Neuroscience and Biomedical Engineering

Supervising professor
Professor Risto Ilmoniemi, Aalto University, Finland

Thesis advisors
Doctor Juha Montonen, BioMag Laboratory, University of Helsinki and Helsinki University Hospital, Finland
Docent Matti Stenroos, Aalto University, Finland

Preliminary examiners
Professor Peter van Leeuwen, University of Witten/Herdecke, Germany
Professor Jari Hyttinen, Tampere University of Technology, Finland

Opponent
Professor Jens Haueisen, Ilmenau University of Technology, Germany

Aalto University publication series
DOCTORAL DISSERTATIONS 106/2017

ISBN 978-952-60-7466-5 (printed)
ISBN 978-952-60-7465-8 (pdf)
ISSN-L 1799-4934
ISSN 1799-4934 (printed)
ISSN 1799-4942 (pdf)
http://urn.fi/URN:ISBN:978-952-60-7465-8

Unigrafia Oy
Helsinki 2017

Finland

441 697
Printed matter

Author
Ville Mäntynen

Name of the doctoral dissertation
The cardiomagnetic field: Non-invasive mapping of atrial fibrillation and model-based characterization of sensitivity and resolution

Publisher School of Science

Unit Department of Neuroscience and Biomedical Engineering

Series Aalto University publication series DOCTORAL DISSERTATIONS 106/2017

Field of research Engineering Physics, Biomedical Engineering

Manuscript submitted 13 June 2017 **Date of the defence** 20 October 2017

Permission to publish granted (date) 28 September 2017 **Language** English

☐ **Monograph** ☒ **Article dissertation** ☐ **Essay dissertation**

Abstract

Atrial fibrillation (AF) is the most common arrhythmia of the heart and a major burden to health care. The prevalence of AF (2%) is increasing with ageing population. Different physiological mechanisms underlying AF as well as increasing options for its treatment call for advancement in diagnostics. One approach is through measurement of the electromagnetic field that the electrochemical activity of the heart gives rise to. In magnetocardiography (MCG), the cardiomagnetic field is measured outside the thorax and analyzed. In this Thesis, I have studied and developed multichannel MCG mapping in order to characterize the cardiac function and AF.

The cardiomagnetic field was studied using non-invasive MCG mappings of healthy subjects and AF patients as well as with computer simulations. To identify and characterize MCG signal features related to AF, the atrial activity was assessed using MCG recorded during both the sinus rhythm and arrhythmia. During the sinus rhythm, the MCG map pattern was shown to depend on the interatrial conduction pathway (CP) as determined by invasive electrophysiological study; an MCG method was developed to assess the CP non-invasively. In another study, MCG map types associated with different CPs were found to occur in different proportions in patients and in healthy subjects. In addition, a technique for assessing the temporal evolution of the MCG map during ongoing arrhythmia was introduced. The technique brought up recurrent spatiotemporal MCG map patterns with abrupt changes and substantial interpatient differences. The techniques developed provide new means for non-invasive characterization of atrial activity and may also be clinically useful.

In the modelling part of this work, spatial properties of MCG, electrocardiography (ECG), and combined MCG+ECG were studied in terms of signal generation charac-teristics and source-estimation performance. These were assessed by amplitudes of simulated signal topographies and characteristics of point-spread functions for sources all around the heart. The results showed that the relative signal amplitude depends not only on the location and orientation of the source but also on the measurement modality, and that this amplitude profile is also reflected to the source estimates. The simulations illustrate the complementary information pro-vided by electro- and magnetocardiography. For optimal sensitivity and resolution, MCG and ECG should be combined.

Keywords magnetocardiography, atrial fibrillation, volume conductor modelling, point-spread function

ISBN (printed) 978-952-60-7466-5 **ISBN (pdf)** 978-952-60-7465-8

ISSN-L 1799-4934 **ISSN (printed)** 1799-4934 **ISSN (pdf)** 1799-4942

Location of publisher Helsinki **Location of printing** Helsinki **Year** 2017

Pages 132 **urn** http://urn.fi/URN:ISBN:978-952-60-7465-8

Tekijä
Ville Mäntynen

Väitöskirjan nimi
Sydämen magneettikenttä: Ei-invasiivinen eteisvärinän kartoitus ja mittauksen herkkyyden ja erotuskyvyn malliperusteinen tarkastelu

Julkaisija Perustieteiden korkeakoulu

Yksikkö Neurotieteen ja lääketieteellisen tekniikan laitos

Sarja Aalto University publication series DOCTORAL DISSERTATIONS 106/2017

Tutkimusala Teknillinen fysiikka, lääketieteellinen tekniikka

Käsikirjoituksen pvm 13.06.2017 **Väitöspäivä** 20.10.2017

Julkaisuluvan myöntämispäivä 28.09.2017 **Kieli** Englanti

☐ **Monografia** ☒ **Artikkeliväitöskirja** ☐ **Esseeväitöskirja**

Tiivistelmä
Eteisvärinä (EV) on yleisin sydämen rytmihäiriö ja se kuormittaa terveydenhuoltoa merkittävästi. Eteisvärinän esiintyvyys (2%) kasvaa jatkuvasti väestön keski-iän nousun myötä. EV:n monimuotoisten syntymekanismien ymmärtämiseksi ja taudin hoitovaihtoehtojen lisääntyessä tarvitaan uusia diagnostisia menetelmiä. Yksi lähestymistapa on sydämen sähkökemiallisen toiminnan aiheuttaman sähkömagneettisen kentän mittaaminen ja tutkiminen. Magnetokardiografiassa (MKG) mitataan sydämen toiminnan aiheuttamaa magneettikenttää kehon ulkopuolelta potilaaseen kajoamatta. Tässä väitöskirjassa olen tutkinut ja kehittänyt monikanavaista MKG-kartoitusmittausta sydämen toiminnan ja EV:n kuvaamiseksi.

Sydämen magneettikenttää tutkittiin terveiden koehenkilöiden ja EV-potilaiden MKG-kartoitusmittausten sekä tietokonesimulaatioiden avulla. EV:ään liittyvien MKG-signaalipiirteiden tunnistamiseksi ja kuvailemiseksi eteistoimintaa tutkittiin sekä normaalin sinus-rytmin että rytmihäiriön aikaisista MKG-mittauksista. Sinus-rytmin aikana MKG-kartan muodon näytettiin riippuvan eteisten välisen aktivaation johtumisreitistä, jonka eri vaihtoehdot ja yhdistelmät määritettiin invasiivisten elektrofysiologisten mittausten avulla; työssä kehitettiin MKG-menetelmä johtumisreitin määrittämiseksi potilaaseen kajoamatta. Menetelmää sovellettiin laajemmassa mittausaineistossa, ja eri johtumisreitteihin liitettyjen MKG-karttatyyppien esiintyvyydessä havaittiin ero potilaiden ja terveiden välillä. Lisäksi esiteltiin menetelmä MKG-kartan aikakäytöksen kuvailemiseksi EV:n aikana. Tällä menetelmä havaittiin toistuvia MKG-karttapiirteitä, niiden äkillisiä muutoksia sekä näiden molempien selviä eroja potilaiden välillä. Kehitetyt menetelmät tarjoavat uusia tapoja tutkia ja kuvailla sydämen eteisten sähköistä toimintaa potilaaseen kajoamatta ja niistä voi olla myös kliinistä hyötyä.

Tämän työn mallinnusosassa tutkittiin monikanavaisen MKG:n, elektrokardiografian (EKG) sekä yhdistetyn MKG+EKG:n spatiaalisia ominaisuuksia signaalin synnyn sekä signaalin synnyttävien lähteiden estimoinnin kannalta. Näitä arvioitiin mallintamalla joka puolelle sydäntä asetettujen lähteiden signaalitopografioiden amplitudeja sekä lähde-estimoinnin pisteenleviämisfunktion piirteitä. Tulokset osoittivat, että suhteellinen signaalinvoimakkuus riippuu lähteen paikan ja orientaation lisäksi mittausmenetelmästä, ja myös lähde-estimaatit riippuvat tästä herkkyysjakaumasta. Mallinnukset havainnollistavat elektro- ja magnetokardiografian antamaa toinen toistaan täydentävää tietoa. MKG:n ja EKG:n tarjoama tieto tulisi yhdistää optimaa-lisen mittausherkkyyden ja lähteiden erotuskyvyn saavuttamiseksi.

Avainsanat magnetokardiografia, eteisvärinä, tilavuusjohdemallinnus, pisteenleviämisfunktio

ISBN (painettu) 978-952-60-7466-5 **ISBN (pdf)** 978-952-60-7465-8

ISSN-L 1799-4934 **ISSN (painettu)** 1799-4934 **ISSN (pdf)** 1799-4942

Julkaisupaikka Helsinki **Painopaikka** Helsinki **Vuosi** 2017

Sivumäärä 132 **urn** http://urn.fi/URN:ISBN:978-952-60-7465-8

Preface

Over the years leading to this Thesis, I have had the privilege to work and carry out research at the BioMag Laboratory, Helsinki University Hospital, and at the Department of Neuroscience and Biomedical Engineering (NBE), Aalto University, Helsinki. The research has received funding from the Aalto University, Academy of Finland (141102), Alfred Kordelin Foundation, Finnish Cultural Foundation, Finnish Foundation for Cardiovascular Research, Helsinki University Hospital, and Instrumentarium Science Foundation; I thank these institutions for their support.

I am grateful to my supervisor Prof. Risto Ilmoniemi, the Head of NBE, for all his support and for the opportunity to finalise this Thesis at the NBE; I thank the Head of BioMag Laboratory, Docent Jyrki Mäkelä, for the measurement facilities and for reserving my desk at BioMag in the meantime. I am much obliged to my instructors Dr. Juha Montonen and Docent Matti Stenroos; from start to finish of this project, their ideas, guidance on scientific thinking and writing, help in finding funding, persistence, and time&willingness for (the occasional motivational) discussion have been indispensable.

I thank my co-authors and devote special thanks to my closest collaborators, Dr. Raija Jurkko, Mr. Teijo Konttila, Dr. Mika Lehto, and Dr. Anne-Mari Vitikainen, with whom I have spent countless hours tinkering many necessary as well as unnecessary details behind the published research. I also thank Docent Markku Mäkijärvi, Dr. Hannu Parikka, and Docent Lauri Toivonen, for their support and for sharing their expertise on cardiology. I thank the preliminary examiners, Prof. Jari Hyttinen and Prof. Peter van Leeuwen for their thorough comments and suggestions to improve the Thesis manuscript; for proofreading and peer support I thank soon-to-be doctors Niko Mäkelä and Lari Koponen.

I acknowledge my former and current colleagues at the BioMag/hospital and NBE for pleasant and productive days at work, and for pleasant, (stimulating, and therefore, hopefully not that) unproductive hours around the coffee table. (Un)fortunately, all my academic as well as non-academic friends that have

somehow contributed to this Thesis, are too numerous to be listed here—I hope a simple “thank you” and a possible coffee&cake will help you defeat the disappointment of not finding your name printed in this fine book.

Over and beyond this Thesis project, I am most grateful to my family for their support, patience, and love. My mother Virpi and my father Erkki are always there when needed, despite the fact that Espoo is located at such a distant periphery, far away from the middle part of Finland. My brother Samuli I thank especially for the motivation-motivated present, a tailcoat. Finally, I cannot thank enough my four beautiful ladies at home, Vilma, Matilda, Minea, and Niina—I love you and from now on, I will try to be a better father and husband, and be more present.

Espoo, September 2017,

Ville Mäntynen

Contents

List of publications

This doctoral dissertation consists of a summary and of the following publications that are referred to in the text by their numerals.

I Mäntynen V, Vitikainen A-M, Koskinen R, Mäkijärvi M, Toivonen L, Montonen J. Magnetocardiography is sensitive to differences in inter-atrial conduction in patients with paroxysmal lone atrial fibrillation. *International Congress Series, volume 1300*, pp. 508–511, 2007.

II Jurkko R, Mäntynen V, Tapanainen JM, Montonen J, Väänänen H, Parikka H, and Toivonen L. Non-invasive detection of conduction pathways to left atrium using magnetocardiography: validation by intra-cardiac electroanatomic mapping. *EP Europace*, volume 11, issue 2, pp. 167–177, 2009.

III Jurkko R, Mäntynen V, Lehto M, Tapanainen JM, Montonen J, Parikka H, Toivonen L. Interatrial conduction in patients with paroxysmal atrial fibrillation and in healthy subjects. *International Journal of Cardiology*, volume 145, issue 3, pp. 455–460, 2010.

IV Mäntynen V, Lehto M, Parikka H, Montonen J. Noninvasive mapping reveals recurrent and suddenly changing patterns in atrial fibrillation: A magnetocardiographic study. *submitted*.

V Mäntynen V, Konttila T, and Stenroos M. Investigations of sensitivity and resolution of ECG and MCG in a realistically shaped thorax model. *Physics in Medicine and Biology*, volume 59, pp. 7141–7158, 2014.

Author's contribution

Publication I Magnetocardiography is sensitive to differences in interatrial conduction in patients with paroxysmal lone atrial fibrillation

The author designed and implemented the spatial interpolation of magnetocardiographic (MCG) signals into magnetic field maps using magnetic multipole expansion. He also further developed and applied the quantification of magnetic field map orientation using field gradients. He is the principal author of the article.

Publication II Non-invasive detection of conduction pathways to left atrium using magnetocardiography: validation by intra-cardiac electroanatomic mapping

The author fine-tuned the methods of Publication I, applied them to pre-processed MCG data, performed the corresponding part of the statistical analysis, and prepared the figures for publication. He took part in interpreting the results and writing the manuscript.

Publication III Interatrial conduction in patients with paroxysmal atrial fibrillation and in healthy subjects

The author participated in recording the MCG data, applied the methods of Publication II to pre-processed MCG data, performed all statistical analysis, and prepared the figures for publication. He took part in interpreting the results and editing the manuscript for publication.

Publication IV Non-invasive mapping reveals recurrent and suddenly changing patterns in atrial fibrillation: A magnetocardiographic study

The author was the main technical investigator. He designed and constructed the analysis framework to study MCG mappings of ongoing atrial fibrillation. He implemented the required additions to the existing signal processing and analysis methods, and analysed the results. He is the principal author of the article.

Publication V Investigations of sensitivity and resolution of ECG and MCG in a realistically shaped thorax model

The author was involved in study design and in implementation of simulation routines. The author conducted the simulations and analysed the results. He is the principal author of the article.

1. Introduction

1.1 Background

The human heart is about fist-sized four-chamber muscle that pumps blood through the circulatory system. Blood carries oxygen and other metabolic substances such as nutrients, hormones, and waste products. The blood from the lungs and the rest of the body enters the heart into the left and the right atria, respectively. The atria feed the blood into the ventricles that in turn pump it back into circulation. The pumping action, i.e., the contraction of cardiac muscle cells is caused by their electrochemical activity. In a healthy heart, an electrical impulse originating from the sinoatrial, i.e., the sinus node spreads as a wavefront through the whole myocardium in an organized manner for optimal pumping of blood; the spread is often called cardiac (electrical) conduction. In a normal cardiac cycle, the electrical activity spreads first through the atria and then through the ventricles, followed by a resting phase so that, in sinus rhythm, the heartbeat is regular. The electrical activity also gives rise to an electromagnetic field that can be measured and analysed to study the function of the heart. In electrocardiography (ECG), the cardiac activity is interpreted from tracings of voltages measured on the body surface; unhealthy function of the heart is often but not always associated with abnormal features in ECG tracings. To arrive at a diagnosis and decide upon medical intervention, ECG interpretations are combined with other diagnostic information such as known risk factors and results from, e.g., ultrasound imaging, blood pressure measurement, and blood tests. ECG is also used for monitoring effects of pharmaceutical or other treatment.

Atrial fibrillation (AF) is the most common arrhythmia (Camm *et al.*, 2010; January *et al.*, 2014). During AF, disorganized electrical impulses cause trembling contraction, i.e., fibrillation of the atria. Rapid atrial activity often induces also fast and irregular (ventricular) heartbeat. Although AF is not immediately life-threatening, it increases the risk of stroke, death, dementia and heart failure. Symptoms of AF reduce the quality of life significantly, and AF patients need frequent hospitalization, burdening the health care system. The preva-

lence of AF (2%) is increasing with ageing population and the number of patients is expected to at least double over the next four decades (Ball *et al.*, 2013). The current as well as the expected burden have driven the research on AF for better understanding of the disease and development of new treatments, both of which call for new or improved diagnostic methods.

The information carried by standard ECG is limited so that more extensive and accurate knowledge about the electrical function of the heart would help in understanding diseases such as AF and thus would also aid clinical decision making. Direct measurement of the cardiac tissue is possible but, being an invasive procedure, is limited in availability and not suitable for, e.g., general screening. New and complementary information on AF is sought using non-invasive multichannel measurements with tens of sensors and an extensive spatial coverage; such an ECG measurement is called body-surface potential mapping (BSPM). In magnetocardiographic (MCG) mapping, the cardiomagnetic field is measured in several locations near the chest without physical contact; the measurement typically covers the anterior chest. Wide spatial coverage and a large number of measurement locations in both MCG and BSP mapping enable and call for new analysis methods: Instead of inspecting the signal tracings directly as is done in traditional ECG analysis, the electric or magnetic field distributions are represented as maps. Features of these maps, such as their shapes and orientations, are then inspected and related with, e.g., information from invasive measurements (Hänninen *et al.*, 2000; van Leeuwen *et al.*, 2011). Prior to the Publications in this Thesis, there were only few studies on AF using MCG. The relationship between ECG and MCG has been debated since the invention of MCG in the 1960s—the value and possible benefits of MCG, or combined MCG+ECG, are still not fully known.

1.2 Aims

In this Thesis, I study and develop the non-invasive magnetocardiographic approach. The objective of this Thesis is to obtain a better understanding of the potential of MCG. The problem is approached experimentally in the setting of atrial fibrillation (AF), and theoretically using computer simulations. The Thesis consists of Publications I–V, with the following aims:

1. To identify and characterize MCG signal features related to AF

   Publication I: To assess the sensitivity of MCG to atrial activation order determined by the interatrial conduction pathway during sinus rhythm.

   Publication II: To identify the interatrial conduction pathways during sinus rhythm non-invasively using MCG.

   Publication III: To explore whether interatrial conduction during sinus rhythm differs between healthy controls and patients with paroxysmal (i.e., episodes of) atrial fibrillation.

   Publication IV: To demonstrate the use of MCG in characterization of ongoing atrial fibrillation.

2. To characterize spatial information carried by multichannel ECG/MCG recordings

   Publication V: To quantify the sensitivity and resolution of ECG, MCG, and combined MCG+ECG systematically for sources all around the heart.

2. Cardiac electromagnetism and atrial fibrillation

In this chapter, the basics of cardiac bioelectromagnetism and multichannel measurements, including cardiac source imaging, are introduced. An overview on AF is given, followed by a brief review of previous ECG and MCG mapping studies on AF.

2.1 Basics of signal generation

The ability of a nerve or a cardiac cell to transport electrical impulses is based on the excitability of the cell membrane and an event called action potential, which is briefly described below; for a textbook reference, see (Gulrajani, 1998). The (cardiac) cell membrane is impermeable to ions but it contains ion channels and pumps that, on one hand, maintain a concentration difference of ions across the membrane and on the other, make it excitable. Because of the ion concentration difference at rest, the cardiac cell membrane is electrically polarized so that the inside of the cell is at a lower potential than the outside. In response to an electrical or electrochemical stimulus, certain ion channels open, causing rapid local *depolarization* on the cell membrane that is then followed by a return to resting state through repolarization; this event is called an action potential. It initiates at a certain level of membrane voltage so that any event that causes the membrane voltage to rise, i.e., depolarize, adequately can act as a stimulus. Locally, the depolarization occurs within milliseconds so that the action potential acts as a stimulus to the neighbouring membrane patch and the depolarization spreads along the membrane as a wavefront. Because the cardiac cells are electrically connected via gap junctions, the depolarization propagates through the whole myocardium as a *wavefront*. The mechanical contraction of the cardiac muscle cells is triggered by the inflow of calcium ions during action potential. In part because of this (depolarizing) ion current, the cardiac muscle cells are refractory (i.e., renewed depolarization is hindered) for a period of about 250 milliseconds after depolarization; this is a

physiological mechanism specific to cardiac cells that allows coordinated mechanical contraction of the heart and pumping of the blood.

The shape and amplitude of the measured ECG or MCG signal tracing depends on the location of the sensor; for example, an activation wavefront that propagates towards (away from) an ECG electrode causes a positive (negative) deflection in the measured signal. To study the function of the heart from measured ECG and MCG signals, we need to relate the electrical activity to the electromagnetic field; this is characterized with a *measurement model*: The cardiac electromagnetic field can be considered to arise from bioelectric sources operating inside a volume conductor. The measurement model describes the sources, the sensors and the transfer of the signal between them. In 1913, Einthoven *et al.* (1913) characterized the mean direction of electrical activation with a two-dimensional vector derived from measurements with three electrodes. This earliest model led to the concept of "heart vector", which is used as a conceptual basis of ECG interpretation still today.

The heart vector is quantitatively represented with an equivalent current dipole. It is the simplest source model and used still today in, e.g., vector cardiography. A single dipole is, however, only a rough approximation to model the whole depolarization wavefront propagating through the heart; more detailed models have been developed. An activation wave propagating in a single cardiac muscle cell can be modelled as a depolarization dipole (Macfarlane and Lawrie, 1989). At tissue level, the depolarization wavefront thus appears as a dipole layer (Gulrajani, 1998): the cellular dipoles at the wavefront lead, on macroscopic scale, to an equivalent source-current density, i.e., distributed dipole-moment density. This source of the electric and magnetic fields, $\boldsymbol{E}$ and $\boldsymbol{B}$, is expressed as primary current density $\boldsymbol{J}_\mathrm{p}$ (Gulrajani, 1998; Nenonen *et al.*, 1994; Sarvas, 1987; Tripp, 1983). The highest significant frequency component of the time varying bioelectromagnetic fields is about 1 kHz, which is related to the action potential rise time (about 1 ms). Thus, in tissue, resistive component dominates over the capacitive component and the field computation is commonly handled using quasi-static Maxwell equations (Plonsey and Heppner, 1967), meaning that any change in source currents is assumed immediately visible in the fields everywhere.

The primary current density $\boldsymbol{J}_\mathrm{p}$ gives rise to a primary charge distribution and electric field $\boldsymbol{E}$ that drives the volume current $\boldsymbol{J}_\mathrm{v} = \sigma\boldsymbol{E} = -\sigma\nabla\phi$, where ϕ is the electric potential, and σ the electric conductivity. The total current is thus $\boldsymbol{J} = \boldsymbol{J}_\mathrm{p} + \boldsymbol{J}_\mathrm{v}$. Due to the conservation of charge, we then get the Poisson equation for potential

$$\nabla \cdot (\sigma \nabla \phi) = \nabla \cdot \boldsymbol{J}_\mathrm{p} \tag{1}$$

This equation describes the *forward problem* of ECG; after solving ϕ, the differences of ϕ on the body surface yield the ECG signals. The magnetic field $\boldsymbol{B}$ is integrated from the Biot–Savart law:

$$\begin{aligned} \boldsymbol{B}(\boldsymbol{r}) &= \frac{\mu_0}{4\pi} \int_{V'} \frac{\left[\boldsymbol{J}_\mathrm{p}(\boldsymbol{r}') + \boldsymbol{J}_\mathrm{v}(\boldsymbol{r}')\right] \times (\boldsymbol{r} - \boldsymbol{r}')}{|\boldsymbol{r} - \boldsymbol{r}'|^3} dV' \\ &= \frac{\mu_0}{4\pi} \int_{V'} \frac{\left[\boldsymbol{J}_\mathrm{p}(\boldsymbol{r}') - \sigma(\boldsymbol{r}')\nabla\phi(\boldsymbol{r}')\right] \times (\boldsymbol{r} - \boldsymbol{r}')}{|\boldsymbol{r} - \boldsymbol{r}'|^3} dV' \end{aligned} \tag{2}$$

where $\boldsymbol{r}$ is the observation point, and the integral is calculated with respect to primed coordinate $\boldsymbol{r}'$ over the whole thorax volume V'; note that ϕ, the solution of (1), is needed in solving the magnetic forward problem. As all currents give rise to a magnetic field, the field measured as MCG consists of two parts: the field generated directly by the primary current density $\boldsymbol{J}_\mathrm{p}$ and the field due to volume current density $\boldsymbol{J}_\mathrm{v}$ (Geselowitz, 1970). Figure 1 shows MCG and BSP maps simulated from a single current dipole.

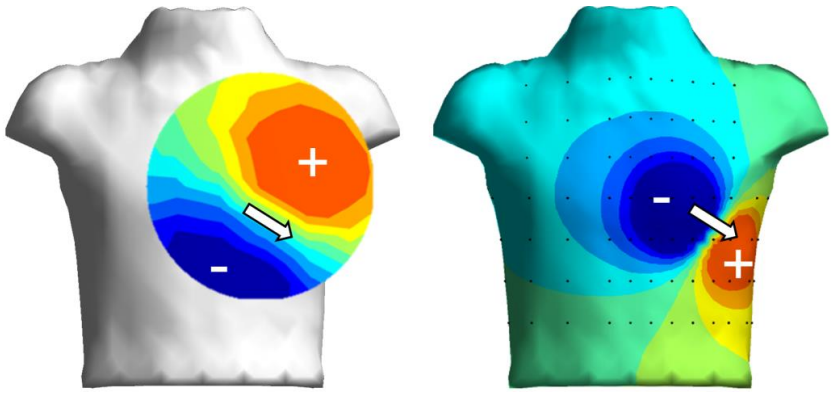

Figure 1. Isocontours of (left) magnetic field component $\boldsymbol{B}_z$ and (right) surface potential due to a tangential current dipole simulated inside a homogeneous thorax. The component $\boldsymbol{B}_z$ points towards the reader, out of the chest in the figure; the current dipole is located near the apex of the heart and illustrated with an arrow. The simulation was performed using models and methods used in Publication V.

2.2 Cardiac activation and surface signal

In a healthy heart, the depolarization propagates as a wavefront through the whole myocardium in an organized manner. The conduction system (figure 2) is specialized cardiac muscle tissue that orchestrates and accelerates the spread of depolarization to ensure timely and organized rhythmic contraction of the heart, i.e., optimal pumping of blood. Cells of the conduction system depolarize spontaneously and are thus capable of firing an action potential. In the healthy heart, however, the cells in the *sinoatrial node (SA)* depolarize the fastest, thus setting the pace; the SA node is often called sinus node and the normal rhythm is called *the sinus rhythm* (SR).

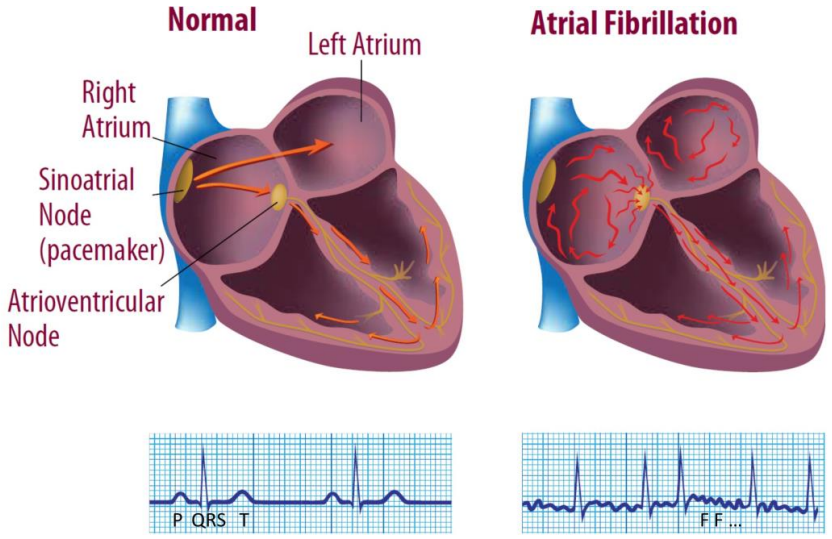

Figure 2. Anatomy and electrical activation of the heart. Normal activation starts periodically at the sinus node, located at the upper part of the wall of the right atrium. The electrical activity spreads as a wavefront; the conduction system (yellow) accelerates and controls the spread of activity. Voltage measurable on the body surface is known as the electrocardiogram (ECG). An ECG tracing shows characteristic signal deflections (PQRST) during normal rhythm. During atrial fibrillation, the electrical activity in the atria is disorganized and unceasing, often inducing fast and irregular ventricular heartbeat; for details, see Section 2.4. Modified from (Centers for Disease Control and Prevention, 2015).

The normal activation order of the human heart follows the conduction system and is illustrated in the left panel of figure 2: In the atria, the depolarization wavefront spreads roughly radially from the sinus node towards the left atrium and down towards the atrioventricular (AV) node, typically following the Bachmann bundle[1] and internodal pathways, respectively. The ventricles are electrically connected to the atria only through the AV node, which also delays the activation to allow the atria contract and fill the ventricles with

[1] The interatrial conduction occurs through different pathways of which the Bachmann bundle is the most common.

blood before they start to contract. From the AV node, the bundle of His and its branches transmit and distribute the activation rapidly to the ventricular tissue. For a more detailed description of depolarization wavefront propagation, see, e.g., (Durrer *et al.*, 1970; Gulrajani, 1998). The normal activation of the heart shows on the ECG as characteristic signal deflections called the *P wave,* the *QRS complex*, and the *T wave*. The P wave reflects the atrial depolarization, whereas the QRS complex and the T wave correspond to the ventricular depolarization and repolarization, respectively. The MCG signal deflections share the naming with the ECG.

2.3 Magnetocardiography

2.3.1 History and background

The cardiomagnetic field was first detected in the early 1960's (Baule and McFee, 1963). When measured outside the thorax, it has a peak amplitude of about 50 pT, which is about one millionth of the Earth's magnetic field and one thousandth of the magnetic noise from man-made structures and machines in urban areas. To minimize the external magnetic disturbances, the early experiments were made outdoors using two copper-wound detector coils connected as a gradiometer, i.e., a device insensitive to the absolute magnetic field strength but sensitive to (a component of) the magnetic field gradient that for far-away sources is presumably very weak. The development of magnetically shielding chambers enabled the use of a magnetometer coil, i.e., the measurement of a component of the actual magnetic field, and MCG recording in a laboratory environment (Cohen, 1967), but recording of real-time MCG with ECG-like clarity became possible only after the invention of the ultrasensitive SQUID[2] sensor (Cohen *et al.*, 1970; Zimmerman and Frederick, 1971). SQUIDs have also enabled magnetoencephalography (MEG), the study of the human brain by measuring its magnetic fields (Hämäläinen *et al.*, 1993; Vrba *et al.*, 2006).

Modern MCG devices typically contain tens of sensors arrayed inside a measurement head. The measurement head, i.e., the sensor array, is positioned at the desired location above thorax, and in some systems it can also be tilted to follow the subject's chest shape. Most MCG devices measure the magnetic field component roughly perpendicular to the chest, denoted as B_z, using sensors installed on a single plane (in some systems, the array surface is slight-

[2] Superconducting quantum interference device; cooled with liquid helium

ly curved) above the supine subject. There is a considerable diversity of measurement systems (Mäkijärvi *et al.*, 2010; Vrba *et al.*, 2006): The measurement can be carried out either inside a magnetically shielded room (MSR) or in an unshielded environment. Depending on the manufacturer and amount of shielding used, the devices differ in the number, type, and layout of individual sensors. The environmental noise is typically reduced with software and in some systems also with reference sensors.

2.3.2 Applications

In clinical research, MCG has been applied mainly to probe ventricular conditions with most of the research concentrating on the diagnosis of ischemia and arrhythmia risk assesment (Kwong *et al.*, 2013; Mäkijärvi *et al.*, 2010). In clinical practice, fetal MCG (fMCG) is an established means to study the heart of an unborn baby, making it perhaps the most important clinical application of MCG so far (Donofrio *et al.*, 2014).

2.3.3 Relationship with ECG

Several experimental studies suggest that MCG and ECG (BSPM) contain complementary information (Brockmeier *et al.*, 1997; Lant *et al.*, 1990; Nakaya *et al.*, 1988; Oostendorp and Pesola, 2001; Takala *et al.*, 2001). Both MCG and ECG arise essentially from the same source, the electrochemical activity of the heart. They are, however, different in terms of the signal generation as well as the measurement—the complementarity of MCG and ECG has been debated since the birth of MCG (Plonsey, 1972; Wikswo Jr, 1983). It has been interpreted that MCG is relatively more sensitive to tangential currents, whereas ECG is more sensitive to radial currents (Vrba *et al.*, 2006; Wikswo Jr, 1983). The “Brody effect” plays a part in this interpretation: well-conducting blood inside the heart enhances the ECG signal due to radial source current (dipole), but attenuates the signal due to tangential source current (Plonsey, 1972; van Dam and van Oosterom, 2005). In addition, a curved primary current (e.g., a train of dipoles or a bent wire) produces a primary magnetic field that is different from the field due to a corresponding straight primary current (with identical ends), whereas their electric fields, i.e., the volume currents are identical (Liehr *et al.*, 2005; Wikswo Jr, 1983).

The differences in the information content between MCG and ECG (BSPM) are still unclear (Kwong *et al.*, 2013; Mäkijärvi *et al.*, 2010). As described earlier, both MCG and ECG signals depend on volume currents, complicating signal interpretation. MCG appears, however, less affected than ECG by thorax

inhomogeneities such as anisotropic skeletal muscles (Pesola *et al.*, 1999). Layer-like structures have only a weak effect on magnetic fields, regardless of their conductivity (Cohen and Hosaka, 1976; Sarvas, 1987), which enables the recording and analysis of fetal MCG with superior signal-to-noise ratio compared to ECG (Donofrio *et al.*, 2014).

MCG is measured without a physical contact, avoiding the electrode contact issues and skin irritation that may arise when using ECG. Issues with relative sensor locations are also absent because of the fixed sensor locations; MCG mapping is reproducible provided that the measurement head position can be accurately repeated (Koskinen *et al.*, 2005). As a consequence, preparations for an MCG measurement can be fast. Because of the cryocooling and magnetic shielding required, setting up an MCG laboratory is, however, very expensive compared to ECG and BSPM. On the other hand, the cost per measurement for BSPM is likely higher when factoring in the cost of electrodes and the preparation time.

A few ECG leads, or the standard 12-lead ECG, are often recorded simultaneously with MCG; recording of simultaneous BSPM is also possible but rarely applied. Obviously, ECG and MCG analysis results can be compared. The simultaneously recorded ECG can be used to link the MCG recording to a recording from another modality at a different time such as the intracardiac data with simultaneous ECG in Publication II.

The spatial sensitivity profile of MCG is another motivation for the AF-related MCG studies (Publications I–IV) in this Thesis: The depolarization wavefront spreads over the atrial tissue largely tangentially (Durrer *et al.*, 1970) while during AF, multiple simultaneous wavefronts may appear vortex-like and circular, i.e., curved, resulting in attenuated ECG. On the other hand, it appears that in the literature, MCG is most often contrasted against rather than combined with other modalities such as ECG (Kwong *et al.*, 2013). Combined MCG+ECG contains more information than either modality alone (Oostendorp and Pesola, 2001) but the added value may be difficult to extract. Like the differences between MCG and ECG, the benefits of combined MCG+ECG are unclear. In Publication V, the modalities are investigated with the help of modelling and analysis of their signal generation and source estimation performance; the publication also attempts to clarify the terms such as “current” and “tangential” that are sometimes vaguely defined, e.g., as above. Terms “tangential” and “radial” sometimes refer to the body surface, as in, e.g., (Wikswo Jr, 1983), and sometimes to the heart surface, as in, e.g., (Plonsey, 1972).

2.4 Atrial fibrillation

In a healthy heart, the signal tracings of successive heartbeats are nearly identical and show a more or less steady pace. During an *arrhythmia*, the electrical activity is abnormal so that either the activation order, rhythm, or both are disturbed. According to the 2014 AHA/ACC/HRS AF Guideline (January *et al.*, 2014):

> *AF occurs when structural and/or electrophysiological abnormalities alter atrial tissue to promote abnormal impulse formation and/or propagation. These abnormalities are caused by diverse pathophysiological mechanisms, such that AF represents a final common phenotype for* ***multiple disease pathways and mechanisms that are incompletely understood****.*

In other words, AF requires an initiating electric stimulus (which are usually called *triggers)* and vulnerable tissue (*substrate*) for maintenance. Currently it is believed that *fibrillatory conduction* in the rest of the atria may be "driven" by rapid focal ectopic activity, such as triggers most often arising from the pulmonary veins, or by re-entrant activity sustained by the substrate itself (Nattel *et al.*, 2017; Woods and Olgin, 2014). The current clinical classification of AF is based on the duration of the arrhythmia (January et al., 2014). The disease often progresses from *paroxysmal*, i.e., brief episodes, to *persistent* form; *lone AF* refers to the absence of evidence about an underlying disease[3]. In general, these classifications have no direct or clear relationship to the underlying mechanisms but as the disease progresses, the tissue is believed to become more vulnerable and thus assume a more important role relative to triggers (Woods and Olgin, 2014). AF is associated with multiple risk factors including old age, hypertension and diabetes but mechanisms behind its initiation and maintenance are not fully understood and are thus actively studied and debated (Hansen *et al.*, 2016).

Clinically, ECG is mainly used for confirming AF diagnosis and for monitoring the ventricular rate in response to treatment. The fibrillatory conduction during AF is illustrated in the right panel of figure 2 as several small depolarization wavefronts wandering around the atria; in such a case, the P waves are replaced by irregular deflections, F waves. When these wandering impulses reach the AV node in its non-refractory state, the ventricles depolarize. This results in irregular timing of QRS complexes that occur simultaneously with

[3] As noted in (January *et al.*, 2014), the descriptor *lone AF* has been applied variably. For clinical background on patients involved in the Publications I–III, see the publications and (Jurkko, 2009)

the F waves at a fast rate. These described changes in the ECG form the basis of AF diagnosis (January *et al.*, 2014).

Current treatment of AF is aimed at symptoms and reducing risk of cardiomyopathy and stroke (Woods and Olgin, 2014). The optimal treatment strategy in a given patient is often not known; in general, the outcome of a treatment varies considerably and more targeted treatments are needed. Currently, considerable research effort is tackling the approaching "epidemic" of AF and AF treatment options are increasing. For example, catheter ablation techniques targeted at abolishing AF drivers are evolving rapidly but conclusive evidence for their efficacy remains unclear so far (Ramirez *et al.*, 2017). New diagnostic methods are needed and developed to learn more about AF and to support novel treatments; for example, intracardiac as well as body-surface potential mappings are expected to help in understanding, e.g., re-entry mechanisms (Nattel *et al.*, 2017). In addition to novel physiological measurements, personalized computer models of AF are another approach under active development (Nattel *et al.*, 2017; Trayanova, 2014). To support clinicians in treatment selection and monitoring the outcome, especially non-invasive methods would be desirable.

Earliest clinical studies on the atrial MCG (P wave) were reported in the 1980s (Sumi *et al.*, 1986; Takeuchi *et al.*, 1988); for feasible recordings of the extremely weak atrial signals (Saarinen *et al.*, 1974), technological advances in reducing the background noise were crucial. Prior to the early 2000s, there were relatively few studies on the atrial MCG (Kandori *et al.*, 2002; Sato *et al.*, 2002; Winklmaier *et al.*, 2009). With globally growing research interest on AF, projects were started also at our institute in Helsinki: In 2003, a pilot study indicated that MCG could be more sensitive than ECG (BSPM) to separate right and left atrial activity (Nenonen *et al.*, 2003). The following reports on measurement reproducibility (Koskinen *et al.*, 2005) and P wave signal characteristics (Jurkko *et al.*, 2008) set up the basis for future studies, i.e., Publications I–IV and (Lehto *et al.*, 2009).

In the beginning of 2000s, three distinct interatrial pathways had been identified invasively in humans (Lemery *et al.*, 2004; Roithinger *et al.*, 1999): the Bachmann bundle (BB), the rim of fossa ovalis (FO), and the coronary sinus ostial region (CS). By potentially providing a substrate for abnormal impulse propagation, it was reasonable to think that these pathways could also relate to susceptibility to AF. At the time, the prolongation and morphological changes of (ECG) P wave had been related to interatrial block (conduction delay) and

susceptibility to AF (Bayés de Luna *et al.*, 1988), but signal features, ECG or MCG, related to distinct interatrial pathways had not been identified.

Over the recent two decades, noninvasive characterization of ongoing AF using ECG has been suggested for, e.g., classifying patients and AF phenotypes, evaluating different treatment strategies, and predicting treatment outcome. The complexity of electrical activity has been linked to the persistence of AF (Allessie *et al.*, 2010; Lee *et al.*, 2014) and predictability of treatment outcome (Meo *et al.*, 2013; Yoshida *et al.*, 2012); the complexity has been characterized using ECG signal parameters such as frequency and entropy (Alcaraz and Rieta, 2010; Bollmann *et al.*, 2006; Lankveld *et al.*, 2014). Most studies have used the traditional 12-lead ECG or a single lead. There is, however, emerging evidence that more could be learned by adding leads outside the spatial coverage of the standard ECG (Lankveld *et al.*, 2014; Meo *et al.*, 2013). For maximal information, body-surface potential mapping (BSPM) with tens of leads around the thorax has been suggested (Cuculich *et al.*, 2010; Guillem *et al.*, 2013; Haissaguerre *et al.*, 2014) and non-invasive mapping of AF using BSPM is gaining wider accecptance (Nattel *et al.*, 2017; Ramirez *et al.*, 2017). So far, MCG has only been applied in a few studies to assess ongoing AF (Yamada *et al.*, 2003; Kim *et al.*, 2007; Nakai *et al.*, 2008; Yoshida *et al.*, 2012).

2.5 Cardiac source imaging

The *inverse problem* of ECG or MCG aims at estimating cardiac electrical activity noninvasively from multichannel ECG or MCG measurements. It is often referred to as source localization or functional source imaging, as it aims at describing spatial distribution/location of the activity and also its time course. This kind of information could contribute to safer and more efficient treatment of patients suffering from, e.g., arrhythmias (Berger *et al.*, 2006; Haissaguerre *et al.*, 2014; Kim *et al.*, 2007). Noninvasive imaging can also be applied in the general population, unlike invasive methods. It could thus help in screening, treatment allocation and monitoring, and in basic research on, e.g., mechanisms of atrial fibrillation (Cuculich *et al.*, 2010; Haissaguerre *et al.*, 2014). The inverse problem of ECG/MCG has been reviewed, e.g., in (Dössel, 2000; MacLeod and Brooks, 1998; Nenonen, 1994; Pullan *et al.*, 2010; Stenroos, 2008).

To solve the inverse problem, the measurements are combined with a mathematical model of the source, sensors, and transfer of the signal, i.e., the measurement model. First, the *forward problem* is solved for a discretized template source distribution. Then, the sources underlying the measured sig-

nals are estimated using this model, additional prior information about the sources, and the measurement. A constraining model of the source distribution is used because the inverse problem is ill-posed with multiple solutions: infinitely many source distributions can produce the same field distribution. In addition, further regularization is usually needed to render the solution stable; for examples, see, e.g., (Horáček and Clements, 1997; Nenonen *et al.*, 2001; van Dam *et al.*, 2009; van Oosterom, 1999).

Sensitivity and point-spread function analysis

Sensitivity and resolution are two important characteristics of any imaging system. In linear systems, these can be studied using computer simulations by measuring amplitudes of simulated signal topographies and by characterizing point-spread functions (PSFs), respectively. A PSF describes the response of a linear imaging system to a point-like elementary source (Backus and Gilbert, 1968; Tarantola, 2005); the response to any source is then a linear combination of PSFs. Point-spread functions can be characterized using simple metrics such as spread and peak position with respect to the true source. Bioelectromagnetic multichannel mappings, such as MCG and BSPM, can be considered as linear imaging systems. In this application, signal topographies are simulated by solving the forward problem for discretized source distribution, i.e., a set of point-like source atoms, whereas the "imaging function" is acquired by solving the linear inverse problem. The sensitivity and PSF analysis have recently been applied in electro- and magnetoencephalography (see, e.g., Molins *et al* 2008, Hauk *et al* 2011, Stenroos and Hauk 2013); in Publication V, they are applied to study spatial properties of multichannel ECG and MCG measurements.

3. Methods in this thesis

3.1 MCG measurement

Magnetocardiograms analyzed in the research reported in this Thesis were recorded at the BioMag Laboratory[4] (Helsinki University Hospital, Finland) in a magnetically shielded room (ETS-Lindgren Euroshield Oy, Eura, Finland) using a 99-channel cardiomagnetometer (Elekta Neuromag Ltd, Helsinki, Finland). The MCG device carries 33 thin-film dc-SQUID triple-sensor units (VTT, Finland), each with one magnetometer and two orthogonal planar gradiometers. The sensor units are arranged on a slightly curved surface (with radius of curvature of 82 cm, following the chest surface) at the bottom of the measurement head that has a diameter of 30 cm. For positioning, the measurement head can be tilted in any direction (about 15 degrees) as well as shifted vertically. The measurement system is also equipped with 64 unipolar ECG channels, part of which can be configured as bipolar. The MCG and ECG signals recorded simultaneously are saved both in a single digital output file.

Preparations for the recording are carried out outside the shielded room. The subject is set lying on a non-magnetic bed, and the ECG electrodes and so-called torso-position indicator (TPI) coils are attached. Locations of these coils along with selected anatomical landmarks and electrodes are digitized (Isotrak II, Polhemus, USA); in the beginning of an MCG recording, the TPI coils are fed with current and the measurement system localizes them.

In the MCG recordings of this Thesis, the center of the measurement head was positioned over the anterior chest 15 cm below the jugular notch and 5 cm left from the midsternal line (Koskinen *et al.*, 2005). The tilt and height adjustments were used to set the measurement head as close as possible to the subject's chest without touching it and ensuring room for breathing. The ECG amplifier was configured for recording the (six) limb leads of the standard 12-lead ECG and bipolar XYZ leads (Breithardt *et al.*, 1991). Each recording lasted

[4] https://www.biomag.hus.fi/

for at least 7 minutes; the signals were sampled at 1000 Hz and the pass-band was set to 0.03–300 Hz.

Magnetocardiograms were recorded from subjects showing various aspects of atrial conduction, summarized here from MCG method-development point of view (see also aims of the studies, Section 1.2): First, MCGs were recorded from patients in sinus rhythm, undergoing electrophysiological examination prior to catherer ablation therapy for symptomatic AF, thus providing invasive reference data on interatrial conduction (Publications I and II). Second, the method developed in Publications I and II was applied on MCG recordings from an age- and gender-matched group of healthy volunteers and symptomatic patients with paroxysmal lone AF (in sinus rhythm, Publication III). Third, MCGs were recorded from patients during ongoing atrial arrhythmia considered to represent atrial arrhythmias typically encountered in clinical practice (Publication IV). The AF research reported in this Thesis is a part of clinical AF research projects between BioMag Laboratory, Helsinki University Hospital, and Aalto University; details on the clinical characteristics and, e.g., criteria of inclusion for the patients studied in Publications II and III are described in more detail in the Publications and in the dissertation of Dr. Jurkko, MD (2009).

3.2 Signal processing

Preprocessing and signal averaging

To increase the signal-to-noise ratio during the atrial (P-wave) waveform, the MCG data recorded during normal (sinus) rhythm were signal-averaged. The possible variability of P-wave morphology within each recording was taken into account by selective averaging (Koskinen *et al.*, 2005): Each candidate P-wave in the recording was matched with a user-selected template P-wave for maximum correlation. The candidate was then either accepted or rejected based on criteria set by the user; these criteria included limits for, e.g., maximum noise deviation and minimum correlation. The template was selected to represent the most common P-wave morphology; in some recordings with alternate frequently occurring P-wave morphologies, these were averaged separately.

Determining time intervals

Time intervals to be studied within the P wave were determined based on P-wave start and end (Koskinen *et al.*, 2005): the onset and offset of the atrial wave were detected automatically for each signal-averaged channel. The medi-

an of the onset times over magnetometer channels was considered the beginning of the (detected) atrial activation and denoted as *P wave start*; the offset times were treated analogously to determine the *P wave end*.

Without signal averaging—ongoing AF

During atrial fibrillation, ECG and MCG signals are irregular and show no electrically silent intervals. The zero level of the signal (baseline) is thus difficult if not impossible to determine accurately during AF. Therefore, atrial-signal averaging and some of the related preprocessing methods cannot be used; in addition, the ceaseless atrial activity "contaminates" the QRST complexes. Consequently, special methods for processing fibrillatory signals have been developed. For example, one may attempt estimating the underlying fibrillatory signal (Stridh and Sornmo, 2001). In Publication IV, signal segments with ventricular activity were discarded (Guillem *et al.*, 2009). The methods used in signal characterization need to tolerate relatively higher amount of noise compared to those used with signal-averaged data. For MCG data in Publication IV, in addition to standard noise suppression techniques (described below), also frequency domain filtering was applied to reduce the baseline drift and measurement noise (Guillem *et al.*, 2009). In addition, the parameterization of an MCG measurement described in the next section can be considered as a dimension reduction to extract a desired feature of the multichannel data while discarding others considered as noise.

Environmental noise suppression and signal reconstruction

In this Thesis, environmental noise in the MCG recordings was reduced using the signal-space projection method (SSP) (Uusitalo and Ilmoniemi, 1997). SSP is widely used with MEG and also routinely used in online monitoring and post processing of the BioMag MCG signals. The signal topographies due to external sources, that are typically far away from the sensors, are confined to a small-dimensional subspace that is nearly orthogonal to the heart signal space and are suppressed with appropriate projection vectors. These vectors are determined from an "empty room" measurement, i.e., a measurement without a subject (e.g., Nurminen, 2014). Since the heart signals are not fully orthogonal to the external signal, the application of SSP distorts sensor signals, which has to be taken into account in source modelling. The original signal waveforms can be partially reconstructed through source modelling (Numminen *et al.*, 1995; Takala *et al.*, 2001).

3.3 Magnetic field map

Magnetic field maps (MFM), as shown in Figure 3, illustrate the spatial distribution of the magnetic field component perpendicular[5] to the measurement surface. They are a common means for visualizing MCG data at fixed time instants. A time interval is evaluated by integrating signals on all channels over the interval to form an integral map; to illustrate the signal mean, this map is normalised by the interval length.

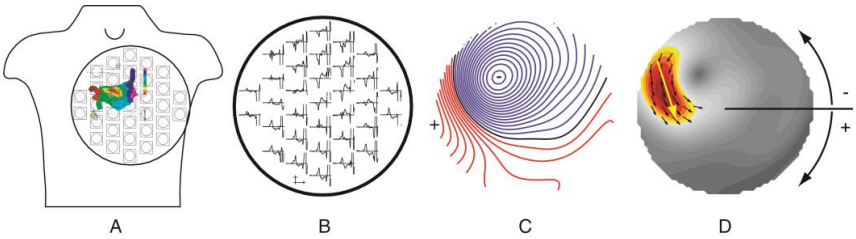

Figure 3. Recording and analysis of atrial magnetic fields. (A) The sensor arrangement, (B) signal-averaged P-waves, (C) MFM over the middle part of P-wave, and (D) the corresponding pseudocurrent map; in (D), the large yellow arrow indicates the magnetic field orientation (MFO), with zero angle direction pointing horizontally from subject's right to left and positive clockwise. From Publication II.

In this Thesis, the MFMs were constructed using magnetic multipole expansion. The method is described in the Appendix of Publication II. Briefly, the magnetic multipole expansion is a mathematical series expansion of the magnetic scalar potential, analogous to the electric multipole expansion (Jackson, 1999); in this Thesis, real spherical harmonic functions were used for the expansion (Karp *et al.*, 1980). The magnetic multipole expansion is based on the assumption that the sensors are confined to a current-free region in space. The coefficients of the expansion can be interpreted as an equivalent source that consists of dipolar, quadrupolar, octapolar, etc. terms. To estimate/interpolate the magnetic field distribution on the sensor surface for visualization, the expansion coefficients are determined from the measured data and then used to compute the magnetic field at desired locations. In the linear measurement model (4), introduced in Section 3.5, vector $\boldsymbol{s}$ then contains the multipole coefficients and $\boldsymbol{L}$ the fields due to unit-strength multipoles; the coefficients can be solved using, e.g., pseudoinverse of $\boldsymbol{L}$ (Nenonen *et al.*, 1994; Sarvas, 1987).

In Publications I–V, MCG sensors were modelled using Neuromag Oy coil descriptions, i.e. locations and weights for numerical integration of the magnetic flux through the sensor pickup-coil (Hämäläinen, 2009). For visualiza-

[5] In BioMag MCG with slightly curved sensor surface, this component is in fact radial but still denoted in the usual manner as $\boldsymbol{B}_z$.

tion on the sensor surface, the magnetic field was in Publications I–IV reconstructed on a regularly spaced grid and in Publication V on the nodes of a triangle mesh.

Orientation of magnetic field map

The orientation of an MFM reflects the mean direction of the electrical activation of the heart (van Leeuwen *et al.*, 2008) and is therefore related to the concept of "the heart vector" (see Figure 1). This interpretation is conceptually valid for a tangential dipole. Because the orientation is usually related to the dipolar component of the magnetic field, which attenuates the slowest with increasing distance from the sources, the deduced orientation is relatively insensitive to the distance between the heart and the MCG sensors (Kandori *et al.*, 2001). Using the MFM orientation for characterization of MCG signals thus has both a physiological and a physical motivation. In practice, the MFM and its orientation are affected by the inhomogeneities of the body, i.e., the volume currents, and the orientation cannot be linked strictly to the tangential component of the heart vector (though, the heart vector is a rather abstract concept that is typically linked to orientation as extracted from ECG recordings, and there is no reason to assume that ECG would be less affected by the body than MCG is). Various methods have been used to measure the MFM orientation (Hänninen *et al.*, 2000; Kandori *et al.*, 2001; van Leeuwen *et al.*, 2008); in general, the measured orientation is determined from the reconstructed MFM (or signals at sensors) and is not strictly based on the dipolar component of the field. Clearly, for successful data analysis, e.g., comparing MCGs of patients and healthy controls, it is not even necessary to directly compare the orientation to the actual mean direction of activation (or heart vector) but rather, the orientation can be treated as an abstract parameter charactering the measurement.

In this Thesis, the orientation of an MFM was quantified based on arrow maps, originally presented by Cohen and Hosaka (1976); the construction of an arrow map is sometimes called pseudocurrent (or Hosaka–Cohen) transformation, while the resulting maps are called pseudocurrent maps. An arrow map is formed from planar gradient vectors of the component $\boldsymbol{B}_z$ as

$$\boldsymbol{a} = \frac{\partial}{\partial x}\boldsymbol{B}_z\hat{\boldsymbol{x}} - \frac{\partial}{\partial x}\boldsymbol{B}_z\hat{\boldsymbol{y}}, \tag{3}$$

i.e., rotating the gradient vectors by 90°; the vectors lie on the sensor surface. Originally, Cohen and Hosaka defined the rotation to help in visual interpretation of an MFM: Arrow maps, and specifically, the strongest vectors in each

map can be used as a rough approximation of the (tangential component of the) underlying source current distribution (Haberkorn *et al.*, 2006).

In this Thesis, the pseudocurrent maps, i.e., the arrow maps were constructed from the MFMs as detailed in the Appendix of Publication II. In each map, the pseudocurrent vectors with relative strength above 70% of the maximum[6] were used for further analysis: their mean direction is defined as the magnetic field orientation (MFO), while the area of the strongest vectors is highlighted on the map visualization (Figure 3). This kind of distribution-based measure of the orientation is more robust against noise than, e.g., that corresponding to the maximum gradient of $\boldsymbol{B}_z$. It also allows for assessing the reliability of the orientation measure visually as well as statistically, as a circular variable (Publication IV); for textbook reference on circular statistics, see, e.g., (Jammalamadaka and SenGupta, 2001; Zar, 1999).

3.4 Electroanatomic mapping

In this Thesis, interatrial conduction is studied using MCG. For this kind of non-invasive study, the invasively measured electrophysiological reference can be considered the gold standard. In Publications I and II, the interatrial conduction pathways were determined from the electroanatomic maps (EAM) of the left atrium (LA) measured with CARTO™ System (Biosense Webster, Inc., Diamond Bar, CA, USA) (Gepstein *et al.*, 1997; Roithinger *et al.*, 1999). Briefly, the system determines the location of a steerable catheter and simultaneously records local electrogram on its tip; by measuring multiple (typically tens of) points, the system reconstructs the 3D geometry with electrophysiological information, such as activation time, superimposed on the anatomy.

The area of the earliest left atrial activity in each EAM was determined visually by an experienced reader (two readers in Publication II). This local activity was then assumed to represent the interatrial conduction pathways as follows. The superior area of LA was considered BB, while the inferoposterior area was considered CS and the septal area between these two was considered FO. A combination of pathways was considered when the earliest activity was observed within 15 ms in two areas and the area in between them was inactive; for details and examples, see Publication I and II.

[6] 80% in Publication I.

3.5 Modelling and point-spread function analysis

The forward problem of MCG is typically solved using the boundary element method (BEM) (Nenonen, 1994; Stenroos *et al.*, 2007; Stenroos and Haueisen, 2008). For numerical computations, the primary current distribution $\boldsymbol{J}_\mathrm{p}$ is discretized into a set of current dipoles, which can be considered as point-like source atoms. The signal topographies due to each one of them are simulated and collected into (columns of) a forward operator $\boldsymbol{L}$ (often called the lead-field matrix); the forward/measument model for signal $\boldsymbol{d}$ is then

$$\boldsymbol{d} = \boldsymbol{L}\boldsymbol{s} + \boldsymbol{n} \tag{4}$$

where $\boldsymbol{s}$ is a vector containing the dipole amplitudes and $\boldsymbol{n}$ is the measurement noise.

In Publication V, the signal topographies were simulated in the sensor geometries of the MCG and BSPM[7] devices at the BioMag Laboratory. The anatomical model is based on the Dalhousie thorax model (Hren *et al.*, 1998), which consists of triangulated surface mesh compartments for the thorax, the lungs, the ventricular epicardium (i.e., the outer surface), and the intra-cardiac blood. The model geometries are shown in Figure 9, in Section 4.5 of this Thesis. The forward problem was solved using in-house BEM tools (Stenroos *et al.*, 2007; Stenroos and Haueisen, 2008).

The PSF analysis requires a linear inverse operator (i.e., source estimator) $\boldsymbol{G}$ such that

$$\boldsymbol{d} = \boldsymbol{L}\boldsymbol{s} + \boldsymbol{n} \rightarrow \hat{\boldsymbol{s}} = \boldsymbol{G}\boldsymbol{d}. \tag{5}$$

For this inverse problem, the well-known minimum-norm estimator provides a solution with minimal constraints (Hämäläinen and Ilmoniemi, 1994; Nenonen *et al.*, 1994). The resolution operator is defined (Tarantola, 2005) as $\boldsymbol{R} = \boldsymbol{G}\boldsymbol{L}$ and its columns are called point-spread functions: applying the inverse operator on the signal topography of one of the point-like source atoms yields the inverse solution, i.e., the "image" of the atom.

The PSF is a general description of an imaging system. As a distribution in the source/image space, it can be visualized just like the signal topographies are visualized in the sensor space; for examples, see Figure 2 in Publication V. Specific features of the PSF are characterized using simple metrics such as its peak position and spread about the true source (Hauk *et al.*, 2011; Liu *et al.*, 2002; Stenroos and Hauk, 2013). These kind of measures, yielding a scalar

[7] For electrode layout description, see, e.g., (Takala *et al.*, 2001)

value for each source atom, are then be visualized as distributions in the source space, allowing the PSF to be assessed as a function of source position.

4. Summary of publications

The publications in this Thesis can be divided to two categories: Publications I–IV are related to clinical AF studies and experimental MCG research, while Publication V deals with modeling and theoretical assessment of multichannel MCG/ECG as an imaging system. The publications are summarized in the following sections with the emphasis on the contribution of the author of this Thesis; the clinical aspects of Publications I–III are described in more detail in the corresponding publications and thoroughly discussed in the doctoral thesis of Raija Jurkko (Jurkko, 2009).

4.1 PI: MCG is sensitive to differences in interatrial conduction

This study assesses the sensitivity of MCG to differences in interatrial conduction pathways (CP) in 12 patients assigned to invasive electrophysiological study and catheter ablation treatment for AF. In each patient, MCG was recorded before the invasive operation, while the CP was determined from the electroanatomic maps (see Section 3.4) recorded in the electrophysiological study prior the ablation treatment. The MCG P wave was signal-averaged as described earlier in Chapter 3 (Koskinen *et al.*, 2005). The correlation between ECG P waves recorded simultaneously with both MCG and EAM was computed to confirm the correspondence of atrial activity in each pair (Vitikainen, 2005); in two patients, two different P wave morphologies were successfully measured with both modalities, resulting in a total of 14 MCG–EAM pairs.

The MCG analysis and results are illustrated in Figure 4. The time interval over the latter half of the P wave was selected to represent the main part of LA activation, based on the EAMs and literature (Lemery *et al.*, 2004). The magnetic field map (MFM) over the interval (integral) was interpolated on the sensor surface using magnetic multipole expansion. The MFM was transformed into a pseudocurrent map and its strongest "current" vectors were used to determine the magnetic field orientation (MFO). These orientations, i.e., the MFOs corresponding to each MCG–EAM pair were then marked on a unit cir-

cle using symbols for CPs determined from the corresponding EAM. The results indicate that the MFO over the time interval of the latter half of the P wave is sensitive to differences in interatrial conduction: group BB appears separate from the others.

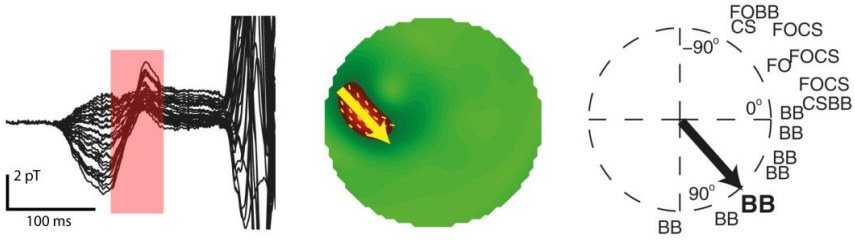

Figure 4. Magnetic field map orientation (MFO) over the latter half of P wave reflects the interatrial conduction pathway. On the left, superimposed P-wave signal averages of magnetometer channels of one patient with the latter half marked with a red box. In the middle, a pseudocurrent map over the interval (on the left) with the large yellow arrow illustrating the mean orientation (i.e., the MFO); the pseudocurrent vectors with the relative amplitude above 80% of the maximum are shown and used to compute the MFO while the underlying color-coding shows their relative amplitudes. On the right, MFOs of all patient MCG–EAM mapping pairs are marked with interatrial conduction pathway symbols: Bachmann bundle (BB), fossa ovalis (FO), and coronary sinus (CS); the symbol corresponding to the MFO of the map in the middle panel is boldfaced and marked with a large arrow; zero angle direction points horizontally from subject's right to left and positive clockwise. Modified from Publication I with permission.

4.2 PII: Identifying interatrial conduction pathways with MCG

A method to identify the interatrial conduction pathways (CP) non-invasively using MCG was developed. To achieve this, several refinements were made to the methods introduced in Publication I; for details, see Publication II and (Jurkko, 2009). MCG and electroanatomic maps (EAM) of atrial activity were recorded in 27 patients presenting diverse interatrial conduction pathways; altogether 29 MCG–EAM pairs pairs were analyzed. The EAMs were interpreted by at least two readers to reach consensus on the CPs.

The MCG maps were divided to three types based on a combination of map orientations (MFOs) corresponding to early and late parts of left atrial (LA) activation (Figure 5); each of these types was related to a distinct interatrial conduction pathway with the help of the corresponding EAM (Figure 6). The mean direction of activation wavefront propagation in each EAM was evaluated visually and compared to the corresponding MCG maps and MFOs. For example, in Figure 5, the early part of the LA activity (green) shows wavefront propagation that is descending, i.e., leftward and down, while towards the later part (purple), the mean direction turns into ascending. Similarly, the (pairs of) MCG maps were separated into three types based on the sign of the MFO, i.e. ascending and descending correspond to negative and positive MFOs, respectively (Figure 6). Using this kind of rough classification, the CP could be de-

termined non-invasively using the MCG map type in 27 out of 29 cases (see also Figure 4 in Publication II).

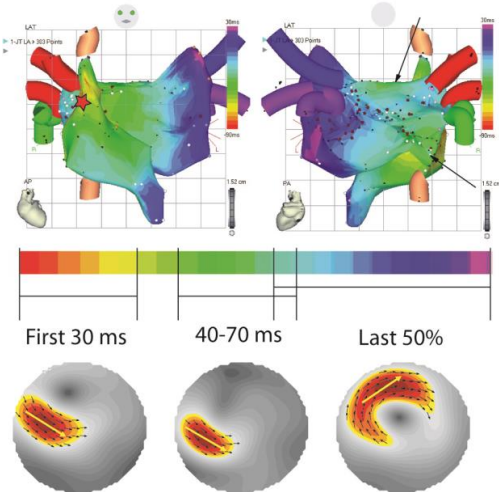

Figure 5. Example of atrial electroanatomic and magnetocardiographic mapping. The EAM (upper row; anterior and posterior views) shows activation isochrones with colour-coded time-scale at 5 ms intervals. The red star marks the earliest right atrial activity, while the arrows point to the two areas of the earliest left atrial activity; in this case, also the right atrium was mapped invasively and the interatrial conduction occurred through both the Bachmann bundle (upper arrow) and coronary sinus (lower) pathways. Modified from Publication II with permission.

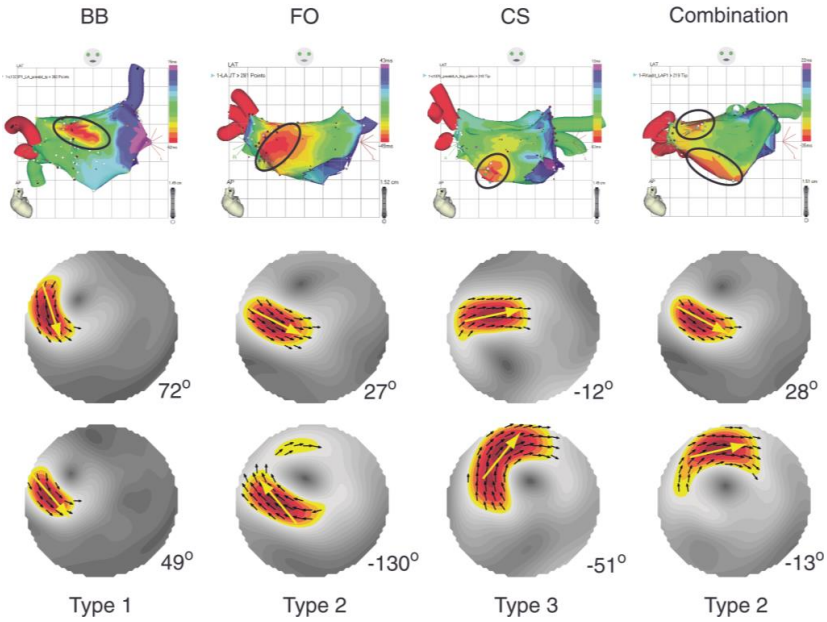

Figure 6. Examples of electroanatomic maps and MCG map types. The top row shows electro-anatomic maps from four cases with different interatrial conduction pathways. The middle and bottom rows show the MCG maps corresponding to the early and late parts of left atrial activation, respectively. The magnetic field map orientation (MFO) is shown next to each map; the type of each map pair is determined from the sign (see Figure 4) of the MFOs as follows: for Type 1, both MFOs are positive; for Type 2, early MFO is positive and late MFO is negative; for Type 3, both MFOs are negative. From Publication II with permission.

4.3 PIII: Interatrial conduction in patients with paroxysmal atrial fibrillation and in healthy subjects

This study applies the MCG map types as categorised in Publication II to examine differences in interatrial conduction between 107 patients with lone paroxysmal atrial fibrillation (AF) and 94 healthy subjects. The duration of atrial waveform in MCG is also assessed. The results show that different MCG map types occur in different proportions in patients in comparison to healthy subjects (Figure 7), suggesting differences in interatrial conduction. The MCG map Type 2, related to conduction via the margin of fossa ovalis or multiple pathways (see Figure 6), was more prevalent in patients. In addition, the results show that there is a high inter-individual variability in the interatrial conduction not only in patients but also in healthy subjects. The duration of the atrial waveform was longer in patients compared to controls only in Type 1 group, which is the type related to conduction via Bachmann bundle. The conclusion was that a collision of electrical impulses via different pathways, in addition to slow conduction, could underlie AF generation.

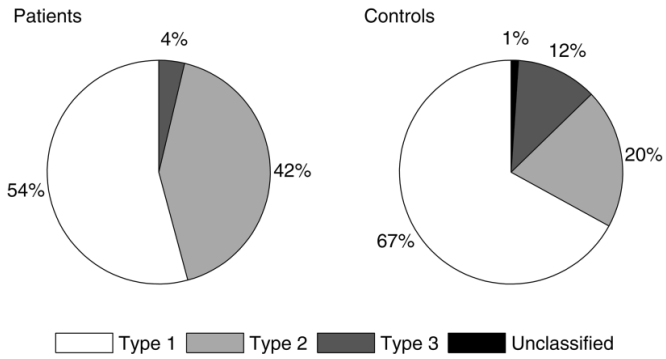

Figure 7. Proportions of different MCG map types in AF patients and in healthy controls. Type 2 is significantly more common in patients than in controls. From Publication III with permission.

4.4 PIV: Characterization of ongoing atrial fibrillation using MCG

This study demonstrates a new approach to characterize ongoing atrial fibrillation using MCG. Nine patients with AF and one with common atrial flutter represented clinically typical atrial arrhythmias. In each patient, MCG with simultaneous ECG was recorded during arrhythmia. An ECG waveform classification based on signal amplitude and regularity was created for reference; each recording was visually inspected by a cardiologist who categorized distinguishable AF segments into four categories; for details, see Publication IV.

Time intervals between QRST complexes were extracted for the analysis; these are referred to as "AF intervals" (Figure 8). Within each AF interval, a sequence of instantaneous MFMs and pseudocurrent maps was computed; for each map, magnetic field orientation (MFO) was computed and its reliability as a mean angle was assessed (Zar, 1999). The consecutive AF intervals and MFO values were then joined as a sequence and the MFO time course of each recording was inspected; the MCG maps were also viewed as animations.

Two examples of the MFO time course are illustrated in Figure 8. The ongoing atrial fibrillation appears in MCG as spatiotemporally organized cyclical sequences, showing rotation of the MCG map. In general, this kind of sequences seem to appear frequently in the recordings whose ECG waveforms were considered as relatively regular. In the recordings with less organized ECG waveforms, also the sequences of rotating MFO appear less frequently and seem to be shorter in duration.

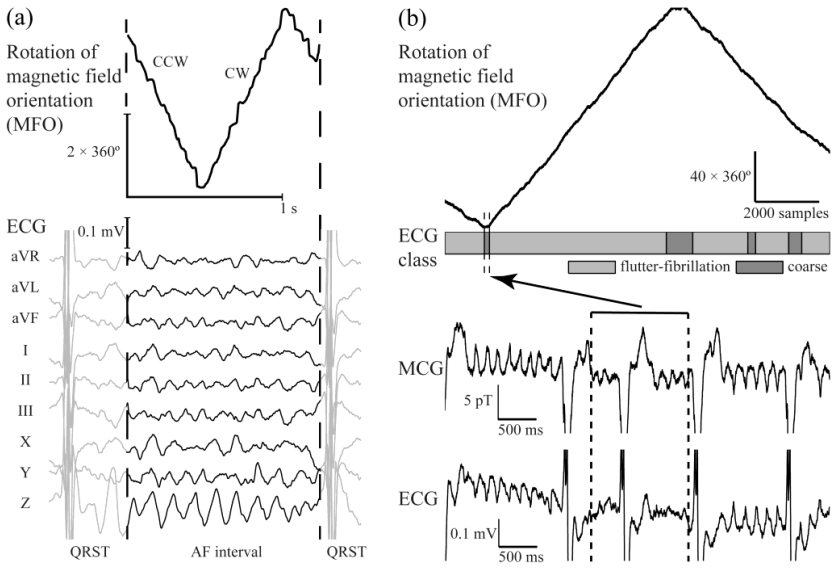

Figure 8. Examples of time courses of the MFO and the concurrent ECG. (a) MFO and ECG waveforms are shown over one AF interval in one patient. In the MFO plot (upper panel), the descending parts indicate counter-clockwise (CCW) and the ascending part clockwise (CW) rotation of the MFO with time; here the rotation changes direction twice within a single AF interval. The concurrent ECG (lower panel) was classified as flutter–fibrillation for the whole period shown. The vertical scale bar in the upper panel indicates rotation corresponding to two full 360-degree cycles (zero angle arbitrary). (b) MFO and the ECG classification (upper panel) are shown over several consecutive AF intervals in another patient; the two changes in the direction of rotation of the MFO co-occur with the first two segments of "coarse AF" in ECG, but during the following two segments of coarse AF, there is no change in rotation. MCG and ECG waveforms (lower panel), including the first segment of coarse AF, seem to change in polarity. From Publication IV.

In Figure 8, the MFO time course reveals transient reversals of the direction of rotation; these were evident also in the corresponding animations. This reversal, presumably arising from the atrial activation sequence, is not immediately

evident in the concurrent ECG or from the orientation (not shown) derived from the ECG. This suggests that MCG may provide both supplementary and complementary information on electrical activity during AF.

To test the idea of enhanced temporal resolution, piecewise linear polynomial function was fitted to the MFO plots, separately on each AF interval; for details, see Publication IV. This enabled automatic tracking and counting of rotation events: *recurrence* was defined as >2 full cycles of consistent rotation, whereas *reversal* of rotation was defined as >1 full cycle of consistent rotation to either direction, followed by >1 full cycle of consistent rotation to the other direction. The slopes of the linear fit corresponding to the recurrence events can be interpreted as frequencies. Although there are significant differences in the computation, the "frequencies" as determined from the slopes were similar to the so-called dominant frequencies of AF reported for MCG (Yoshida *et al.*, 2015). Publication IV puts forward a novel MCG method to characterize the ongoing atrial fibrillation with high temporal resolution.

4.5 PV: Sensitivity profiles and point-spread functions of ECG and MCG

In Publication V, the sensitivity and point-spread function (PSF) of ECG, MCG, and combined ECG+MCG are investigated. This involves volume-conductor modelling and finding the forward and inverse operators, which were briefly introduced in Section 3.5 of this Thesis; the model geometries are shown in Figure 9; the details of the applied methods are described in the Publication.

In published brain studies, PSF analysis has been applied to scalar-valued sources, i.e., sources with fixed orientation (Hauk *et al.*, 2011; Liu *et al.*, 2002; Stenroos and Hauk, 2013). In this work, the analysis was extended to (vector-valued) freely-oriented sources: The source was modelled as a freely-oriented primary current distribution inside the ventricular myocardium. For numerical computations, the source was discretized into a set of unit-amplitude dipoles placed in the vertices of the epicardial surface mesh, as illustrated in Figure 9. The orientation of the three orthogonal dipoles in each vertex was fixed to the local surface geometry so that here "tangential" and "normal/radial" sources refer to the heart surface. Signal topographies for each dipole in each vertex were simulated using BEM (Stenroos *et al.*, 2007; Stenroos and Haueisen, 2008).

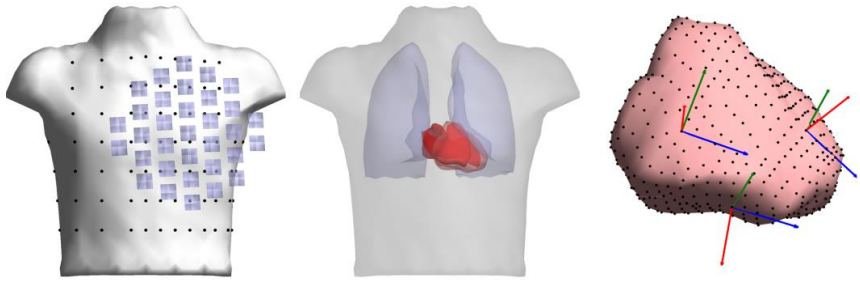

Figure 9. The model geometry. On left, MCG sensors and anterior BSPM electrodes. In the middle, the anterior view of the anatomical model consisting of triangulated surface mesh compartments for the thorax, the lungs, the ventricular epicardium (i.e., the outer surface), and the intra-cardiad blood. On the right, the source locations (black dots) on the surface mesh of the ventricles; example source triplets are shown with red arrow corresponding to the normal ($\boldsymbol{n}$), blue to the first tangential ($\boldsymbol{t}_1$), and green to the second tangential ($\boldsymbol{t}_2$) basis vector orientation. From Publication V.

The inverse problem was solved using minimum-norm estimation (Lin *et al.*, 2006; van Oosterom, 1999); prior the inversion, the forward operator was transformed into signal-to-noise basis through a whitening-like scaling (Fuchs *et al.*, 1998; Oostendorp and Pesola, 2001). This allows combining measurements with different sensor types, such as magnetometers and gradiometers or MCG and ECG, in a single estimate.

The resolution operator was computed as a product of inverse and forward operators yielding PSFs as its columns. Each PSF was measured against the true source (atom) using metrics of localization error (LE) (Lin *et al.*, 2006; Stenroos and Hauk, 2013), spatial deviation (SD) (Stenroos and Hauk, 2013), and orientation error (OE), which is a new metric for vector-valued sources. The signal strength, defined as sensitivity (Se), was measured as the L2-norm of scaled topographies. An example is shown in Figure 10. In the publication, the metrics are visualized as distributions in the source space, allowing the PSF and sensitivity to be studied as functions of source position and orientation.

The results show that the relative signal amplitude depends not only on the measurement modality but also on the location and orientation of the source, and that the sensitivity distribution is clearly reflected in the PSF. MCG excels with anterior tangential sources, while ECG sees overall better the normally-oriented and posterior sources. The sensitivity of combined ECG+MCG is less dependent on source orientation per source location, leading to clearly improved source estimates.

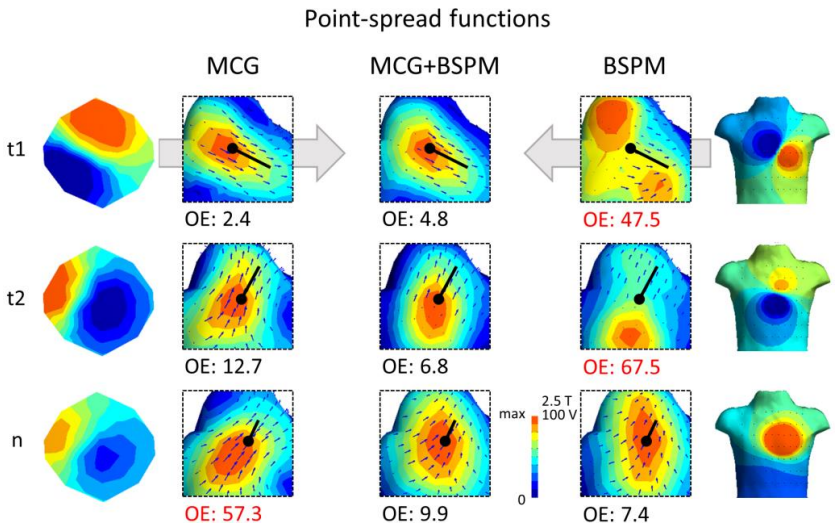

Figure 10. Signal topographies and point-spread functions for three source orientations (black bars) at one location (black dot). The color scaling for PSF amplitude is shown on the left side of the scale bar; the same color bar is used for the signal topographies with symmetric scaling about zero and only (positive) maximums are given. The orientations of PSF/estimate components are illustrated with small arrows and measured with respect to the true source as the orientation error (OE), shown below each PSF; the OE value of 0 corresponds to parallel and value of 100 to orthogonal orientation of the PSF/estimate components in comparison to the true source. The relative magnitudes of the other metrics can be roughly deduced from the figure: Sensitivity corresponds to the amplitude of the signal topography. LE is the distance between the true source and the center-of-mass of the PSF/estimate. SD is the spatial deviation of the PSF/estimate about the true source. Modified from Publication V.

5. Discussion

5.1 Temporal and spatial resolution of MCG and ECG

Magnetocardiography and electrocardiography are physiological measurement modalities with excellent temporal resolution. The spatial resolution of MCG and ECG is, however, limited, because on or above the body surface the magnetic field and electric potential topographies due to neighbouring cardiac sources are very similar and generally widely spread; thus, the signals at sensors close to each other are not independent. In principle, a single MCG or ECG signal tracing does not carry any spatial information—spatial interpretation, e.g., where does the signal comes from, relies on assumptions and knowledge about the signal generation, i.e., the measurement model (see Section 2.1) and prior knowledge about the activity. Signals can be interpreted also without geometrical information, based on prior knowledge about the timing and features of signal waveforms related to specific activity. For example, the heart rate can be determined almost everywhere on the body by detecting consecutive QRS complexes.

In practice, the temporal and spatial capabilities of MCG (or ECG) are connected through the mechanisms of signal generation. The ability to detect small temporal changes in the signal depends on the spatial sensitivity of the measurement. For example, determining the onset of atrial activation (P wave) depends on the strength of signal (above noise) arising in the part of the atria with earliest activation. Similarly, the ability to resolve two events in a measurement depends on their temporal as well as spatial relationship. For instance, we know that the P wave and the QRS complex reflect the atrial and ventricular depolarization, respectively, but during atrial fibrillation, distinguishing the atrial signal component from simultaneous QRS complexes is challenging. In this Thesis, the spatiotemporal capabilities of multichannel MCG were studied and utilized in experimental research on atrial fibrillation (PI–IV), whereas the signal generation and the spatial properties of multi-

channel MCG and ECG (BSPM) were studied and clarified through modelling (PV).

5.2 MCG metrics

The signal features of MCG and ECG are generally characterized using various metrics such as durations and amplitudes of the measured waveforms. MCG and ECG are, however, different in terms of signal generation (see Section 2.1 and PV) so that, in general, the same metrics cannot be assumed to be useful in both modalities; for example, to detect ischaemia with MCG, magnetic field map orientation should be used instead of the ST segment amplitude, which is an ECG standard (Takala, 2001; Takala *et al.*, 2001). Multichannel metrics based on spatial features of the magnetic field map, such as its orientation, incorporate the spatial relationships between the sensors in a natural way so that the actual physical magnetic field is characterized. The magnetic field map, in turn, can be reconstructed through (equivalent) source modelling such as the magnetic multipole expansion used in this Thesis. By explaining the data with multipole coefficients, the data is transformed to device-independent space, which could also be utilized when comparing measurements from different devices (Burghoff *et al.*, 2000). Also other metrics in addition to the orientation should be considered. For example, magnetic field map has been characterized using principal component analysis to compute its relative non-dipolar content (van Leeuwen *et al.*, 2011); a corresponding metric can be computed directly from magnetic multipole coefficients.

In this Thesis, the magnetic field map orientation (MFO) is computed as the mean of thresholded pseudocurrent transformation of reconstructed magnetic field map. Such a process is very tolerant to measurement noise, as was demonstrated by the Publication IV, where no signal-averaging was used. The pseudocurrent transformation resonates with the concept of ECG heart vector, which may help in interpretating and communicating the results—one should, however, bear in mind that the pseudocurrent distribution is not a direct projection of the underlying source current distribution.

As explained in Section 3.3, the orientation values (i.e., angles) computed from the magnetic field maps can be treated as abstract variables to characterize the measurement. Assuming normal distribution in case of circular data may lead to wrong conclusions; the fact that simple arithmetic mean does not always give correct mean orientation seems well recognized in MCG literature. Nevertheless, it appears that in Publications I–III of this Thesis, the orientation was in MCG context treated statistically as a circular variable for the first

time. The use of circular statistics enables the statistical assessment of, e.g., the significance of the computed mean (i.e. the MFO in PIV), and separation and angular–angular correlation between two groups of orientation samples (PIII).

5.3 Implications from experimental studies (PI–IV)

Publications I–III present development and application of an MCG method to detect the interatrial conduction pathways non-invasively. The conclusion that "not only slow conduction but collision of electrical impulses via different routes could underlie AF generation" is still supported by the literature: The usefulness of P-wave duration in AF risk assessment is considered limited (Fuster *et al.*, 2011), whereas the link between AF and interatrial blocks, i.e., altered conduction pathways, has been demonstrated (Bayés de Luna *et al.*, 2012; Conde *et al.*, 2015). Furthermore, abnormal P-wave morphology in ECG, found using a similar classification method, has been found predictive of AF development (Holmqvist *et al.*, 2008, 2010). As pointed out by Conde et al. (2015), the MCG method presented in this Thesis could be useful in early detection of interatrial blocks, but further validation would be needed; it is likely that a better non-invasive separation of interatrial conduction pathways could be found by adjusting the classification (MFO) limits, or by using some other MCG or MCG+ECG metrics altogether. This would require, however, a considerably larger amount of invasive measurements for reference, which are generally not easily attainable.

Short-time dynamics of AF are largely unexplored non-invasively (Alcaraz *et al.*, 2012). Arguably though, the atrial activation patterns can be estimated using cardiac source imaging (Haissaguerre *et al.*, 2014), but such approach demands individual anatomical models, typically acquired using computer tomography, and extensive modelling including restrictive assumptions on the activity (see Section 2.5). To the author's knowledge, Publication IV is the first study to quantitatively assess the temporal evolution of MCG map pattern during ongoing atrial fibrillation. The publication suggests a new means to characterize AF in almost real time enabling the detection of sudden changes in the time course of MCG map that are likely linked to dynamics of atrial fibrillation: invasive studies have described transient spatial organization with very similar temporal behaviour (Haissaguerre *et al.*, 2014; Lee *et al.*, 2014). Because the recording of an invasive reference simultaneously with MCG is very difficult if not impossible, the value of the method and suggested metrics should be evaluated, e.g., in a group of patients assigned to catheter ablation

for treatment of AF. Typical ECG-based measures, such as the dominant frequency, are constructed using signal segments lasting for 10 seconds (Lankveld *et al.*, 2014), while the angular velocity of MFO (rotation) can be estimated from just a few rotations within a couple of hundred milliseconds. Obviously, by condensing multichannel data over a short sampling interval into a single metric, we can detect and quantify instantaneous phenomena in the time course of the feature that the metric describes. This could be used to study, e.g., P-to-P wave variability, which is another largely unexplored subject.

5.4 Implications from the modelling study (PV)

Publication V supports the earlier interpretation from experimental studies that MCG and ECG contain complementary information (Brockmeier *et al.*, 1997; Lant *et al.*, 1990; Oostendorp and Pesola, 2001; Takala *et al.*, 2001). The models, the methods, and the results of the work are discussed rather extensively in the Publication; here, main points are summarized and some additional aspects are discussed.

The freely-oriented primary current distribution can be regarded as the most general and, at the same time, fair source model in this kind of analysis: It is capable of explaining any measured MCG and ECG topography but curved or other electrically silent, and thus MCG-favouring, sources are not explicitly modelled. Still, benefits of adding MCG to ECG were found, which is in line with the results of Oostendorp and Pesola (2001) who used a source model that can be considered ECG-favouring.

The point-spread function is a general description of an imaging system. PSF analysis can be used to study the volume-conductor modelling errors (Stenroos and Hauk, 2013) and properties of different linear estimators such as weighted or surface Laplacian-regularized minimum-norm estimator (Nenonen *et al.*, 2001). In addition, PSF and sensitivity analysis could be used in planning studies. For example, combining MCG with ECG for simultaneous recording in a way that the convenience of MCG recording retains, while adding ECG leads to benefit from the combination[8]. Or the opposite, given that there are ECG methods to assess interatrial block, we could try modelling the interatrial conduction and estimate whether replacing or combining ECG with MCG is worth the trouble and costs. Also sensor system or positioning could

[8] Adding more leads after a certain number does not yield more information; see Publication V and (Oostendorp and Pesola, 2001; Ryynänen *et al.*, 2006).

be designed so that the information is maximized, e.g., atomic magnetometers (Iivanainen *et al.*, 2017; Morales *et al.*, 2017).

Publication V concentrates on basic spatial properties of MCG and ECG. One of the issues to be studied in the future is the required resolution and fidelity of the source model. For optimal added value from MCG, the anisotropic conduction properties of the myocardium may also need to be taken into account in the source model, in addition to volume conduction: experimental studies on so-called bidomain properties indicate possible differences in sources of MCG and ECG (Holzer *et al.*, 2004; McBride *et al.*, 2010). Modelling studies, such as (Wang *et al.*, 2010), should include magnetic field computation to reveal possible benefits of combining the measurements. However, there appears to be gaps in the models and knowledge on how to simulate MCG from electrophysiologically detailed heart models; the author is not aware of any thorough theory+simulation paper on MCG signal generation in anisotropic bidomain, or of any heart model whose MCG would be validated against measurement. Also additional far- and near-field measurements are needed.

5.5 Combining MCG and ECG (PV)

Publication V shows that to optimally benefit from the complementarity of MCG and ECG, the modalities should be combined; this is in line with earlier studies (Korhonen *et al.*, 2002; Oostendorp and Pesola, 2001). In practice, combining MCG and ECG is not straightforward. For simultaneous recording, adding ECG to an existing MCG system is easier and much less expensive than vice versa; in MCG systems, at least a couple of leads, or standard 12-lead ECG is usually already available but adding tens of leads for body surface potential mapping may require an overhaul of the data acquisition system. For combined data analysis, there are at least three foreseeable ways: combining MCG and ECG metrics (Korhonen *et al.*, 2002), using combined MCG+ECG (or both separately) in cardiac source imaging (Oostendorp and Pesola, 2001), or computing combined metrics by treating MCG+ECG as a general multidimensional data set, e.g., like MCG is treated in (Steinisch *et al.*, 2013). In cardiac source imaging, modelling brings a significant part of information to the process, in addition to the measurement. As discussed above and in Section 4.2 in Publication V, volume-conductor modelling errors, the effect of noise, and the required model resolution/fidelity with MCG or combined MCG+ECG should be studied in the future. In addition, modern (e.g., Bayesian) inversion techniques have not, in general, been applied to MCG, let alone combined MCG+ECG (Ahrens *et al.*, 2013).

Combined MCG+ECG is likely to improve, e.g., atrial source estimates, especially in case of atrial fibrillation, where estimating fractionated activity demands high spatial resolution (Zhou *et al.*, 2016). Atrial walls are thin and the activation wavefront propagates mainly tangentially, which together reduce the signal amplitude, i.e., cause a stronger Brody effect compared to the ventricles (van Dam and van Oosterom, 2005). On the other hand, MCG is relatively more sensitive to the tangential source currents (Publication V). The atria are, however, located deeper inside the thorax so that the sensitivity of MCG is lower compared to the ventricles on the average, and also MCG is affected by the Brody effect to some extent. To what extent adding MCG to ECG, or vice versa, helps in studying the atria is currently unknown and should be studied, e.g., with sensitivity and PSF analysis, or by combining experimental results from the modalities.

5.6 MCG misconceptions and future implications

Magnetocardiogram arises from bioelectric current sources embedded inside the human body that acts as volume conductor. There is a common misinterpretation that MCG would not be sensitive to volume currents. The misinterpretation originates in the early MCG studies with results and rules-of-thumb that have been heavily, and also correctly, used in measurement, analysis and interpretation of both MCG and MEG: Bioelectric sources were modelled using current dipoles embedded inside simplified volume conductor geometries (for the body), i.e., the semi-infinite conducting space and conducting sphere, both mathematically as well as by constructing physical approximations (Cohen and Hosaka, 1976). For any source current, specific volume conductor geometries used in early studies are “transparent” to the magnetic field component perpendicular (i.e., normal/radial) to the volume conductor surface, while the other components receive contribution from the volume currents (Sarvas, 1987). Because of symmetry, however, these same geometries are completely non-transparent to source current component perpendicular to the surface, i.e., “radial dipole does not produce any magnetic field”. While in realistic geometries orientations “normal/radial” and “tangential” become obscured, the magnetic field characteristics described above for simplified volume conductors do not cease to exist, but are rather similarly blurred as illustrated, e.g., in Publication V. For example, unlike the interpretation of the results of Publication V in (Morales *et al.*, 2017), for each source location there is a ”radial” source orientation in the sense that the other (orthogonal) source orientations produce relatively stronger magnetic field, and the magnetic field component

tangential to the body surface receives the most contribution from the volume currents (Iivanainen *et al.*, 2017).

Another risk of misinterpretation, to the opposite direction, are biased comparisons. For example, comparing the performance of ECG and MCG in ischemia detection using ST segment amplitude, which is an ECG metric, is likely to give unfavorable MCG result (e.g., Potyagaylo *et al.*, 2015), as discussed earlier and indicated by Takala *et al.* (2001). Similarly, it has been argued that the MCG of normal (healthy) ventricular depolarization can be derived from the BSPM (van Oosterom *et al.*, 1990), which seems to hold with the assumptions used in that study (see Publication V). Nevertheless, the equivalent double-layer source formulation used in that study contains all ECG information (within its validity), but it cannot fully explain MCG, i.e., the possibility of independent information (McBride *et al.*, 2010; Wikswo Jr, 1983).

The research should concentrate on added value and complementary information of MCG in combination with other modalities instead of finding superiority or inferiority. This Thesis studies atrial fibrillation (AF), which is the most common arrhythmia of the heart and a major burden to health care. Improved methods for AF prevention and management are needed, but the underlying mechanisms of the disease are incompletely understood; currently, considerable research effort focuses on AF. There are remarkably few MCG studies on AF, although MCG is well-suited to probing atrial electrical activity and it could, in theory, provide complementary information. Non-invasive mapping of so-called rotors, characterized by circular re-entrant activity during AF (Nattel *et al.*, 2017), should be attempted also using MCG; moreover, non-invasive mapping could probably benefit from combining body-surface potential mapping, applied currently, with simultaneous MCG. On the other hand, e.g., relatively fast allocation of further examination or treatment based on MCG results would be possible because an MCG measurement without simultaneous ECG can be made fast; arguably though, criteria for such allocation do not exists yet and additional measurements and research is needed, perhaps using methods presented in this Thesis. To facilitate the adoption of MCG, as well as the interpretation of MCG in general, computer modelling studies of cardiac electrical function and AF (Trayanova, 2014) in particular, should include computation of MCG in addition to ECG. These approaches could potentially increase our understanding on not only MCG but also atrial fibrillation.

References

Ahrens, H., Argin, F. and Klinkenbusch, L. (2013) Comparison of the extended kalman filter and the unscented Kalman filter for magnetocardiography activation time imaging, *Advances in Radio Science*, 11, pp. 341–346. DOI:10.5194/ars-11-341-2013.

Alcaraz, R., Hornero, F., Martínez, A. and Rieta, J. J. (2012) Short-time regularity assessment of fibrillatory waves from the surface ECG in atrial fibrillation, *Physiological Measurement*, 33 (6), pp. 969–984. DOI:10.1088/0967-3334/33/6/969.

Alcaraz, R. and Rieta, J. J. (2010) A review on sample entropy applications for the non-invasive analysis of atrial fibrillation electrocardiograms, *Biomedical Signal Processing and Control*, 5 (1), pp. 1–14. DOI:10.1016/j.bspc.2009.11.001.

Allessie, M. A., de Groot, N. M. S., Houben, R. P. M., Schotten, U., Boersma, E., Smeets, J. L. and Crijns, H. J. (2010) Electropathological substrate of longstanding persistent atrial fibrillation in patients with structural heart disease: longitudinal dissociation., *Circulation: Arrhythmia and Electrophysiology*, 3 (6), pp. 606–615. DOI:10.1161/CIRCEP.109.910125.

Backus, G. and Gilbert, F. (1968) The resolving power of gross earth data, *Geophysical Journal of the Royal Astronomical Society*, 16 (2), pp. 169–205. DOI:10.1111/j.1365-246X.1968.tb00216.x.

Ball, J., Carrington, M. J., McMurray, J. J. V. and Stewart, S. (2013) Atrial fibrillation: Profile and burden of an evolving epidemic in the 21st century, *International Journal of Cardiology*, 167 (5), pp. 1807–1824. DOI:10.1016/j.ijcard.2012.12.093.

Baule, G. and McFee, R. (1963) Detection of the magnetic field of the heart, *American Heart Journal*, 66 (1), pp. 95–96. DOI:10.1016/0002-8703(63)90075-9.

Bayés de Luna, A., Cladellas, M., Oter, R., Torner, P., Guindo, J., Martí, V., Rivera, I. and Iturralde, P. (1988) Interatrial conduction block and retrograde activation of the left atrium and paroxysmal supraventricular tachyarrhythmia, *European Heart Journal*, 9 (10), pp. 1112–1118.

Bayés de Luna, A., Platonov, P., Cosio, F. G., Cygankiewicz, I., Pastore, C., Baranowski, R., *et al.* (2012) Interatrial blocks. A separate entity from left atrial enlargement: a consensus report, *Journal of Electrocardiology*, 45 (5), pp. 445–451. DOI:10.1016/j.jelectrocard.2012.06.029.

Berger, T., Fischer, G., Pfeifer, B., Modre, R., Hanser, F., Trieb, T., *et al.* (2006) Single-beat noninvasive imaging of cardiac electrophysiology of ventricular preexcitation., *Journal of the American College of Cardiology*, 48 (10), pp. 2045–2052. DOI:10.1016/j.jacc.2006.08.019.

Bollmann, A., Husser, D., Mainardi, L., Lombardi, F., Langley, P., Murray, A., *et al.* (2006) Analysis of surface electrocardiograms in atrial fibrillation: techniques, research, and clinical applications., *EP Europace*, 8 (11), pp. 911–926. DOI:10.1093/europace/eul113.

Breithardt, G., Cain, M. E., El-Sherif, N., Flowers, N. C., Hombach, V., Janse, M., Simson, M. B. and Steinbeck, G. (1991) Standards for analysis of ventricular late potentials using high-resolution or signal-averaged electrocardiography: A statement by a task force committee of the European Society of Cardiology, the American Heart Association, and the American College of Cardiology, *Journal of the American College of Cardiology*, 17 (5), pp. 999–1006. DOI:10.1016/0735-1097(91)90822-Q.

Brockmeier, K., Schmitz, L., Bobadilla Chavez, J. D., Burghoff, M., Koch, H., Zimmermann, R. and Trahms, L. (1997) Magnetocardiography and 32-lead potential mapping: repolarization in normal subjects during pharmacologically induced stress, *Journal of Cardiovascular Electrophysiology*, 8 (6), pp. 615–626. DOI:10.1111/j.1540-8167.1997.tb01824.x.

Burghoff, M., Nenonen, J., Trahms, L. and Katila, T. (2000) Conversion of magnetocardiographic recordings between two different multichannel SQUID devices, *IEEE Transactions on Biomedical Engineering*, 47 (7), pp. 869–875. DOI:10.1109/10.846680.

Camm, A. J., Kirchhof, P., Lip, G. Y. H., Schotten, U., Savelieva, I., Ernst, S., *et al.* (2010) Guidelines for the management of atrial fibrillation: The task force for the management of atrial fibrillation of the European Society of Cardiology (ESC), *EP Europace*, 12 (10), pp. 1360–1420. DOI:10.1093/europace/euq350.

Centers for Disease Control and Prevention (2015) Atrial Fibrillation Fact Sheet|Data & Statistics|DHDSP|CDC. Available from: https://www.cdc.gov/dhdsp/data_statistics/fact_sheets/fs_atrial_fibrillation.htm [Accessed 26 May 2017].

Cohen, D. (1967) Magnetic fields around the torso: production by electrical activity of the human heart, *Science*, 156 (3775), pp. 652–654. DOI:10.1126/science.156.3775.652.

Cohen, D., Edelsack, E. A. and Zimmerman, J. E. (1970) Magnetocardiograms taken inside a shielded room with a superconducting point-contact magnetometer, *Applied Physics Letters*, 16 (7), pp. 278–280. DOI:10.1063/1.1653195.

Cohen, D. and Hosaka, H. (1976) Part II magnetic field produced by a current dipole, *Journal of Electrocardiology*, 9 (4), pp. 409–417. DOI:10.1016/S0022-0736(76)80041-6.

Conde, D., Seoane, L., Gysel, M., Mitrione, S., Bayés de Luna, A. and Baranchuk, A. (2015) Bayés' syndrome: the association between interatrial block and supraventricular arrhythmias, *Expert Review of Cardiovascular Therapy*, 13 (5), pp. 541–550. DOI:10.1586/14779072.2015.1037283.

Cuculich, P. S., Wang, Y., Lindsay, B. D., Faddis, M. N., Schuessler, R. B., Damiano, R. J., Li, L. and Rudy, Y. (2010) Noninvasive characterization of epicardial activation in humans with diverse atrial fibrillation patterns., *Circulation*, 122 (14), pp. 1364–1372. DOI:10.1161/CIRCULATIONAHA.110.945709.

Donofrio, M. T., Moon-Grady, A. J., Hornberger, L. K., Copel, J. A., Sklansky, M. S., Abuhamad, A., *et al.* (2014) Diagnosis and treatment of fetal cardiac disease, *Circulation*, 129 (21), pp. 2183–2242. DOI:10.1161/01.cir.0000437597.44550.5d.

Dössel, O. (2000) Inverse problem of electro- and magnetocardiography: review and recent progress, *International Journal of Bioelectromagnetism*, 2 (2). Available from: https://www.ijbem.org/volume2/number2/doessel/paper_ijbem.htm [Accessed 20 May 2017].

Durrer, D., van Dam, R. T., Freud, G. E., Janse, M. J., Meijler, F. L. and Arzbaecher, R. C. (1970) Total excitation of the isolated human heart., *Circulation*, 41 (6), pp. 899–912. DOI:doi: 10.1161/01.CIR.41.6.899.

Einthoven, W., Fahr, G. and Waart, A. de (1913) Über die Richtung und die manifeste Grösse der Potentialschwankungen im menschlichen Herzen und über den Einfluss der Herzlage auf die Form des Elektrokardiogramms, *Pflüger's Archiv für die gesamte Physiologie des Menschen und der Tiere*, 150 (6–8), pp. 275–315. DOI:10.1007/BF01697566.

Fuchs, M., Wagner, M., Wischmann, H.-A., Köhler, T., Theißen, A., Drenckhahn, R. and Buchner, H. (1998) Improving source reconstructions by combining bioelectric and biomagnetic data, *Electroencephalography and Clinical Neurophysiology*, 107 (2), pp. 93–111. DOI:10.1016/S0013-4694(98)00046-7.

Fuster, V., Rydén, L. E., Cannom, D. S., Crijns, H. J., Curtis, A. B., Ellenbogen, K. A., *et al.* (2011) 2011 ACCF/AHA/HRS focused updates incorporated into the ACC/AHA/ESC 2006 guidelines for the management of patients with atrial fibrillation, *Circulation*, 123 (10), pp. e269–e367. DOI:10.1161/CIR.0b013e318214876d.

Gepstein, L., Hayam, G. and Ben-Haim, S. A. (1997) A novel method for nonfluoroscopic catheter-based electroanatomical mapping of the heart, *Circulation*, 95 (6), pp. 1611–1622. DOI:10.1161/01.CIR.95.6.1611.

Geselowitz, D. (1970) On the magnetic field generated outside an inhomogeneous volume conductor by internal current sources, *IEEE Transactions on Magnetics*, 6 (2), pp. 346–347. DOI:10.1109/TMAG.1970.1066765.

Guillem, M. S., Climent, A. M., Castells, F., Husser, D., Millet, J., Arya, A., Piorkowski, C. and Bollmann, A. (2009) Noninvasive mapping of human atrial fibrillation., *Journal of Cardiovascular Electrophysiology*, 20 (5), pp. 507–513. DOI:10.1111/j.1540-8167.2008.01356.x.

Guillem, M. S., Climent, A. M., Millet, J., Arenal, Á., Fernández-Avilés, F., Jalife, J., Atienza, F. and Berenfeld, O. (2013) Noninvasive localization of maximal frequency sites of atrial fibrillation by body surface potential mapping, *Circulation: Arrhythmia and Electrophysiology*, 6 (2), pp. 294–301. DOI:10.1161/CIRCEP.112.000167.

Gulrajani, R. M. (1998) *Bioelectricity and Biomagnetism*. New York: Wiley.

Haberkorn, W., Steinhoff, U., Burghoff, M., Kosch, O., Morguet, A. and Koch, H. (2006) Pseudo current density maps of electrophysiological heart, nerve or brain function and their physical basis, *BioMagnetic Research and Technology*, 4, pp. 5. DOI:10.1186/1477-044X-4-5.

Haissaguerre, M., Hocini, M., Denis, A., Shah, A. J., Komatsu, Y., Yamashita, S., *et al.* (2014) Driver domains in persistent atrial fibrillation, *Circulation*, 130 (7), pp. 530–538. DOI:10.1161/CIRCULATIONAHA.113.005421.

Hämäläinen, M. (2009) MNE software user's guide. Available from: http://www.martinos.org/meg/manuals/MNE-manual-2.7.pdf [Accessed 3 May 2017].

Hämäläinen, M., Hari, R., Ilmoniemi, R. J., Knuutila, J. and Lounasmaa, O. V. (1993) Magnetoencephalography—theory, instrumentation, and applications to noninvasive studies of the working human brain, *Reviews of Modern Physics*, 65 (2), pp. 413–497. DOI:10.1103/RevModPhys.65.413.

Hämäläinen, M. S. and Ilmoniemi, R. J. (1994) Interpreting magnetic fields of the brain: minimum norm estimates, *Medical & Biological Engineering & Computing*, 32 (1), pp. 35–42. DOI:10.1007/BF02512476.

Hänninen, H., Takala, P., Mäkijärvi, M., Montonen, J., Korhonen, P., Oikarinen, L., Nenonen, J., Katila, T. and Toivonen, L. (2000) Detection of exercise-induced myocardial ischemia by multichannel magnetocardiography in single vessel coronary artery disease, *Annals of Noninvasive Electrocardiology*, 5 (2), pp. 147–157. DOI:10.1111/j.1542-474X.2000.tb00380.x.

Hansen, B. J., Csepe, T. A., Zhao, J., Ignozzi, A. J., Hummel, J. D. and Fedorov, V. V. (2016) Maintenance of atrial fibrillation, *Circulation: Arrhythmia and Electrophysiology*, 9 (10). DOI:10.1161/CIRCEP.116.004398.

Hauk, O., Wakeman, D. G. and Henson, R. (2011) Comparison of noise-normalized minimum norm estimates for MEG analysis using multiple resolution metrics, *NeuroImage*, 54 (3), pp. 1966–1974. DOI:10.1016/j.neuroimage.2010.09.053.

Holmqvist, F., Husser, D., Tapanainen, J. M., Carlson, J., Jurkko, R., Xia, Y., *et al.* (2008) Interatrial conduction can be accurately determined using standard 12-lead electrocardiography: validation of P-wave morphology using electroanatomic mapping in man., *Heart Rhythm*, 5 (3), pp. 413–418. DOI:10.1016/j.hrthm.2007.12.017.

Holmqvist, F., Platonov, P. G., McNitt, S., Polonsky, S., Carlson, J., Zareba, W., Moss, A. J. and for the MADIT II Investigators (2010) Abnormal P-wave morphology is a predictor of atrial fibrillation development and cardiac death in MADIT II patients, *Annals of Noninvasive Electrocardiology*, 15 (1), pp. 63–72. DOI:10.1111/j.1542-474X.2009.00341.x.

Holzer, J. R., Fong, L. E., Sidorov, V. Y., Wikswo Jr, J. P. and Baudenbacher, F. (2004) High resolution magnetic images of planar wave fronts reveal bidomain properties of cardiac tissue, *Biophysical Journal*, 87 (6), pp. 4326–4332. DOI:10.1529/biophysj.104.049163.

Horáček, B. M. and Clements, J. C. (1997) The inverse problem of electrocardiography: a solution in terms of single- and double-layer sources on the epicardial surface, *Mathematical Biosciences*, 144 (2), pp. 119–154. DOI:10.1016/S0025-5564(97)00024-2.

Hren, R., Stroink, G. and Horácek, M. (1998) Spatial resolution of body surface potential maps and magnetic field maps: a simulation study applied to the identification of ventricular pre-excitation sites., *Medical and Biological Engineering and Computing*, 36 (2), pp. 145–157. DOI:10.1007/BF02510736.

Iivanainen, J., Stenroos, M. and Parkkonen, L. (2017) Measuring MEG closer to the brain: Performance of on-scalp sensor arrays, *NeuroImage*, 147, pp. 542–553. DOI:10.1016/j.neuroimage.2016.12.048.

Jackson, J. D. (1999) *Classical Electrodynamics*. 3rd ed. John Wiley & Sons, Inc.

Jammalamadaka, S. R. and SenGupta, A. (2001) *Topics in circular statistics*. Vol. 5. World Scientific Publishing Company. Available from: https://ebookcentral.proquest.com/lib/aalto-ebooks/detail.action?docID=1679584

January, C. T., Wann, L. S., Alpert, J. S., Calkins, H., Cigarroa, J. E., Cleveland, J. C., *et al.* (2014) 2014 AHA/ACC/HRS Guideline for the management of patients with atrial fibrillation a report of the American College of Cardiology/American Heart Association Task Force on Practice Guidelines and the Heart Rhythm Society, *Circulation*, 130 (23), pp. e199–e267. DOI:10.1161/CIR.0000000000000041.

Jurkko, R. (2009, June 12) *Atrial Electric Signal During Sinus Rhythm in Lone Paroxysmal Atrial Fibrillation* (PhD Thesis). University of Helsinki, Helsinki, Finland. Available from : https://helda.helsinki.fi/handle/10138/22812

Jurkko, R., Väänänen, H., Mäntynen, V., Kuusisto, J., Mäkijärvi, M. and Toivonen, L. (2008) High-resolution signal-averaged analysis of atrial electromagnetic characteristics in patients with paroxysmal lone atrial fibrillation., *Annals of Noninvasive Electrocardiology*, 13 (4), pp. 378–385. DOI:10.1111/j.1542-474X.2008.00255.x.

Kandori, A., Hosono, T., Kanagawa, T., Miyashita, S., Chiba, Y., Murakami, M., Miyashita, T. and Tsukada, K. (2002) Detection of atrial-flutter and atrial-fibrillation waveforms by fetal magnetocardiogram, *Medical and Biological Engineering and Computing*, 40 (2), pp. 213. DOI:10.1007/BF02348127.

Kandori, A., Kanzaki, H., Miyatake, K., Hashimoto, S., Itoh, S., Tanaka, N., Miyashita, T. and Tsukada, K. (2001) A method for detecting myocardial abnormality by using a total current-vector calculated from ST-segment deviation of a magnetocardiogram signal, *Medical and Biological Engineering and Computing*, 39 (1), pp. 21–28. DOI:10.1007/BF02345262.

Karp, P. J., Katila, T. E., Saarinen, M., Siltanen, P. and Varpula, T. T. (1980) The normal human magnetocardiogram. II. A multipole analysis., *Circulation Research*, 47 (1), pp. 117–130. DOI:10.1161/01.RES.47.1.117.

Kim, D., Kim, K., Lee, Y.-H. and Ahn, H. (2007) Detection of atrial arrhythmia in superconducting quantum interference device magnetocardiography; preliminary result of a totally-noninvasive localization method for atrial current mapping, *Interactive CardioVascular and Thoracic Surgery*, 6 (3), pp. 274–279. DOI:10.1510/icvts.2006.142869.

Korhonen, P., Tierala, I., Simelius, K., Väänänen, H., Mäkijärvi, M., Nenonen, J., Katila, T. and Toivonen, L. (2002) Late QRS activity in signal-averaged magnetocardiography, body surface potential mapping, and orthogonal ECG in postinfarction ventricular tachycardia patients, *Annals of Noninvasive Electrocardiology*, 7 (4), pp. 389–398. DOI:10.1111/j.1542-474X.2002.tb00190.x.

Koskinen, R., Lehto, M., Väänänen, H., Rantonen, J., Voipio-Pulkki, L.-M., Mäkijärvi, M., Lehtonen, L., Montonen, J. and Toivonen, L. (2005) Measurement and reproducibility of magnetocardiographic filtered atrial signal in patients with paroxysmal lone atrial fibrillation and in healthy subjects, *Journal of Electrocardiology*, 38 (4), pp. 330–336. DOI:10.1016/j.jelectrocard.2005.03.012.

Kwong, J. S. W., Leithäuser, B., Park, J.-W. and Yu, C.-M. (2013) Diagnostic value of magnetocardiography in coronary artery disease and cardiac arrhythmias: A review of clinical data, *International Journal of Cardiology*, 167 (5), pp. 1835–1842. DOI:10.1016/j.ijcard.2012.12.056.

Lankveld, T. A. R., Zeemering, S., Crijns, H. J. G. M. and Schotten, U. (2014) The ECG as a tool to determine atrial fibrillation complexity, *Heart*, 100 (14), pp. 1077–1084. DOI:10.1136/heartjnl-2013-305149.

Lant, J., Stroink, G., ten Voorde, B., Horáček, B. M. and Montague, T. J. (1990) Complementary nature of electrocardiographic and magnetocardiographic data in patients with ischemic heart disease, *Journal of Electrocardiology*, 23 (4), pp. 315–322. DOI:10.1016/0022-0736(90)90121-H.

Lee, G., Kumar, S., Teh, A., Madry, A., Spence, S., Larobina, M., *et al.* (2014) Epicardial wave mapping in human long-lasting persistent atrial fibrillation: transient rotational circuits, complex wavefronts, and disorganized activity, *European Heart Journal*, 35 (2), pp. 86–97. DOI:10.1093/eurheartj/eht267.

Lehto, M., Jurkko, R., Parikka, H., Mäntynen, V., Väänänen, H., Montonen, J., Voipio-Pulkki, L.-M., Toivonen, L. and Laine, M. (2009) Reversal of atrial remodeling after cardioversion of persistent atrial fibrillation measured with magnetocardiography., *Pacing and Clinical Electrophysiology*, 32 (2), pp. 217–223. DOI:10.1111/j.1540-8159.2008.02205.x.

Lemery, R., Soucie, L., Martin, B., Tang, A. S. L., Green, M. and Healey, J. (2004) Human study of biatrial electrical coupling, *Circulation*, 110 (15), pp. 2083–2089. DOI:10.1161/01.CIR.0000144461.83835.A1.

Liehr, M., Haueisen, J., Goernig, M., Seidel, P., Nenonen, J. and Katila, T. (2005) Vortex shaped current sources in a physical torso phantom, *Annals of Biomedical Engineering*, 33 (2), pp. 240–247. DOI:10.1007/s10439-005-8983-6.

Lin, F.-H., Belliveau, J. W., Dale, A. M. and Hämäläinen, M. S. (2006) Distributed current estimates using cortical orientation constraints, *Human Brain Mapping*, 27 (1), pp. 1–13. DOI:10.1002/hbm.20155.

Liu, A. K., Dale, A. M. and Belliveau, J. W. (2002) Monte Carlo simulation studies of EEG and MEG localization accuracy, *Human Brain Mapping*, 16 (1), pp. 47–62. DOI:10.1002/hbm.10024.

Macfarlane, P. W. and Lawrie, T. D. V. (1989) *Comprehensive electrocardiology: theory and practice in health and disease*. Pergamon Press.

MacLeod, R. S. and Brooks, D. H. (1998) Recent progress in inverse problems in electrocardiology, *IEEE Engineering in Medicine and Biology Magazine*, 17 (1), pp. 73–83. DOI:10.1109/51.646224.

Mäkijärvi, M., Korhonen, P., Jurkko, R., Väänänen, H., Siltanen, P. and Hänninen, H. (2010) Magnetocardiography, in: Macfarlane, P. W., van Oosterom, A., Pahlm, O., Kligfield, P., Janse, M., and Camm, J. (eds.) *Comprehensive Electrocardiology*. Springer Science & Business Media,4,.

McBride, K. K., Roth, B. J., Sidorov, V. Y., Wikswo, J. P. and Baudenbacher, F. J. (2010) Measurements of transmembrane potential and magnetic field at the apex of the heart., *Biophys J*, 99 (10), pp. 3113–3118. DOI:10.1016/j.bpj.2010.08.040.

Meo, M., Zarzoso, V., Meste, O., Latcu, D. G. and Saoudi, N. (2013) Spatial variability of the 12-lead surface ECG as a tool for noninvasive prediction of catheter ablation outcome in persistent atrial fibrillation, *IEEE Transactions on Bio-Medical Engineering*, 60 (1), pp. 20–27. DOI:10.1109/TBME.2012.2220639.

Molins, A., Stufflebeam, S. M., Brown, E. N. and Hämäläinen, M. S. (2008) Quantification of the benefit from integrating MEG and EEG data in minimum L2-norm estimation, *NeuroImage*, 42 (3), pp. 1069–1077. DOI:10.1016/j.neuroimage.2008.05.064.

Morales, S., Corsi, M.-C., Fourcault, W., Bertrand, F., Cauffet, G., Gobbo, C., *et al.* (2017) Magnetocardiography measurements with ^{4}He vector optically pumped magnetometers at room temperature, *Physics in Medicine & Biology*, 62 (18), pp. 7267–7279. DOI:10.1088/1361-6560/aa6459.

Nakai, K., Oka, T., Okabayashi, H., Tsuboi, J., Fukuhiro, Y., Fukushima, A., Suwabe, A., Itoh, M. and Yoshizawa, M. (2008) Three-dimensional spectral map of atrial fibrillation by a 64-channel magnetocardiogram., *Journal of Electrocardiology*, 41 (2), pp. 123–130. DOI:10.1016/j.jelectrocard.2007.06.008.

Nakaya, Y., Takeuchi, A., Nii, H., Katayama, M., Nomura, M., Fujino, K., Saito, K. and Mori, H. (1988) Isomagnetic maps in right ventricular overloading, *Journal of Electrocardiology*, 21 (2), pp. 168–173. DOI:10.1016/S0022-0736(88)80013-X.

Nattel, S., Xiong, F. and Aguilar, M. (2017) Demystifying rotors and their place in clinical translation of atrial fibrillation mechanisms, *Nature Reviews Cardiology*, advance online publication. DOI:10.1038/nrcardio.2017.37.

Nenonen, J., Montonen, J. and Koskinen, R. (2003) Surface gradient analysis of atrial activation from magnetocardiographic maps, *International Journal of Bioelectromagnetism*, 5 (1), pp. 98–99.

Nenonen, J., Pesola, K., Hänninen, H., Lauerma, K., Takala, P., Mäkelä, T., *et al.* (2001) Current-density estimation of exercise-induced ischemia in patients with multivessel coronary artery disease, *Journal of Electrocardiology*, 34 (4, Part B), pp. 37–42. DOI:10.1054/jelc.2001.28824.

Nenonen, J. T. (1994) Solving the inverse problem in magnetocardiography, *IEEE Engineering in Medicine and Biology Magazine*, 13 (4), pp. 487–496. DOI:10.1109/51.310989.

Nenonen, J. T., Hämäläinen, M. S. and Ilmoniemi, R. J. (1994) Minimum-norm estimation in a boundary-element torso model, *Medical and Biological Engineering and Computing*, 32 (1), pp. 43–48. DOI:10.1007/BF02512477.

Numminen, J., Ahlfors, S., Ilmoniemi, R., Montonen, J. and Nenonen, J. (1995) Transformation of multichannel magnetocardiographic signals to standard grid form, *IEEE Transactions on Biomedical Engineering*, 42 (1), pp. 72–78. DOI:10.1109/10.362916.

Nurminen, J. (2014) *The magnetostatic multipole expansion in biomagnetism: applications and implications* (PhD Thesis). Aalto University, Helsinki, Finland. Available from : https://aaltodoc.aalto.fi:443/handle/123456789/13324

Oostendorp, T. and Pesola, K. (2001) Non-invasive determination of the activation sequence of the heart based on combined ECG and MCG measurements, in: *Proceedings of the 12th International Conference on Biomagnetism*. Espoo, Finland: Helsinki University of Technology, pp. 813–820.

Pesola, K., Nenonen, J., Fenici, R., Lötjönen, J., Mäkijärvi, M., Fenici, P., *et al.* (1999) Bioelectromagnetic localization of a pacing catheter in the heart., *Physics in Medicine & Biology*, 44 (10), pp. 2565–2578. DOI:10.1088/0031-9155/44/10/314.

Plonsey, R. (1972) Capability and limitations of electrocardiography and magnetocardiography, *IEEE Transactions on Biomedical Engineering*, BME-19 (3), pp. 239–244. DOI:10.1109/TBME.1972.324123.

Plonsey, R. and Heppner, D. B. (1967) Considerations of quasi-stationarity in electrophysiological systems, *The Bulletin of Mathematical Biophysics*, 29 (4), pp. 657–664. DOI:10.1007/BF02476917.

Potyagaylo, D., Seemann, G., Schulze, W. H. and Dössel, O. (2015) Magnetocardiography did not uncover electrically silent ischemia in an in-silico study case, in: *2015 Computing in Cardiology Conference (CinC)*. pp. 1145–1148.

Pullan, A. J., Cheng, L. K., Nash, M. P., Ghodrati, A., MacLeod, R. and Brooks, D. H. (2010) The Inverse Problem of Electrocardiography, in: Macfarlane, P. W., Oosterom, A. van, Pahlm, O., Kligfield, P., Janse, M., and Camm, J. (eds.) *Comprehensive Electrocardiology*. Springer London, pp. 299–344.

Ramirez, F. D., Birnie, D. H., Nair, G. M., Szczotka, A., Redpath, C. J., Sadek, M. M. and Nery, P. B. (2017) Efficacy and safety of driver-guided catheter ablation for atrial fibrillation: A systematic review and meta-analysis, *Journal of Cardiovascular Electrophysiology*. DOI:10.1111/jce.13313.

Roithinger, F. X., Cheng, J., SippensGroenewegen, A., Lee, R. J., Saxon, L. A., Scheinman, M. M. and Lesh, M. D. (1999) Use of electroanatomic mapping to delineate transseptal atrial conduction in humans, *Circulation*, 100 (17), pp. 1791–1797. DOI:10.1161/01.CIR.100.17.1791.

Ryynänen, O. R. M., Hyttinen, J. A. K. and Malmivuo, J. A. (2006) Effect of measurement noise and electrode density on the spatial resolution of cortical potential distribution with different resistivity values for the skull, *IEEE Transactions on Biomedical Engineering*, 53 (9), pp. 1851–1858. DOI:10.1109/TBME.2006.873744.

Saarinen, M., Karp, P. J., Katila, T. E. and Siltanen, P. (1974) The magnetocardiogram in cardiac disorders, *Cardiovascular Research*, 8 (6), pp. 820–834. DOI:10.1093/cvr/8.6.820.

Sarvas, J. (1987) Basic mathematical and electromagnetic concepts of the biomagnetic inverse problem, *Physics in Medicine and Biology*, 32 (1), pp. 11–22. DOI:10.1088/0031-9155/32/1/004.

Sato, M., Terada, Y., Mitsui, T., Miyashita, T., Kandori, A. and Tsukada, K. (2002) Visualization of atrial excitation by magnetocardiogram, *The International Journal of Cardiovascular Imaging*, 18 (4), pp. 305–312. DOI:10.1023/A:1015597910933.

Steinisch, M., Torke, P. R., Haueisen, J., Hailer, B., Grönemeyer, D., Van Leeuwen, P. and Comani, S. (2013) Early detection of coronary artery disease in patients studied with magnetocardiography: An automatic classification system based on signal entropy, *Computers in Biology and Medicine*, 43 (2), pp. 144–153. DOI:10.1016/j.compbiomed.2012.11.014.

Stenroos, M. (2008) *Boundary element method in spatial characterization of the electrocardiogram* (PhD Thesis). Helsinki University of Technology, Helsinki, Finland. Available from : https://aaltodoc.aalto.fi:443/handle/123456789/4538

Stenroos, M. and Haueisen, J. (2008) Boundary element computations in the forward and inverse problems of electrocardiography: comparison of collocation and Galerkin weightings, *IEEE Transactions on Biomedical Engineering*, 55 (9), pp. 2124–2133. DOI:10.1109/TBME.2008.923913.

Stenroos, M. and Hauk, O. (2013) Minimum-norm cortical source estimation in layered head models is robust against skull conductivity error., *Neuroimage*, 81, pp. 265–272. DOI:10.1016/j.neuroimage.2013.04.086.

Stenroos, M., Mäntynen, V. and Nenonen, J. (2007) A Matlab library for solving quasi-static volume conduction problems using the boundary element method, *Computer Methods and Programs in Biomedicine*, 88 (3), pp. 256–263. DOI:10.1016/j.cmpb.2007.09.004.

Stridh, M. and Sornmo, L. (2001) Spatiotemporal QRST cancellation techniques for analysis of atrial fibrillation, *IEEE Transactions on Biomedical Engineering*, 48 (1), pp. 105–111. DOI:10.1109/10.900266.

Sumi, M., Takeuchi, A., Katayama, M., Fukuda, Y., Nomura, M., Fujino, K., Murakami, M., Nakaya, Y. and Mori, H. (1986) Magnetocardiographic P waves in normal subjects and patients with mitral stenosis, *Japanese Heart Journal*, 27 (5), pp. 621–633. DOI:10.1536/ihj.27.621.

Takala, P. (2001) *Cardiac exercise studies with bioelectromagnetic mapping* (PhD Thesis). Helsinki University of Technology, Helsinki, Finland.

Takala, P., Hänninen, H., Montonen, J., Mäkijärvi, M., Nenonen, J., Oikarinen, L., Simelius, K., Toivonen, L. and Katila, T. (2001) Magnetocardiographic and electrocardiographic exercise mapping in healthy subjects., *Annals of Biomedical Engineering*, 29 (6), pp. 501–509. DOI:10.1114/1.1376388.

Takeuchi, A., Watanabe, K., Nomura, M., Ishihara, S., Sumi, M., Murakami, M., Saito, K., Nakaya, Y. and Mori, H. (1988) The P wave in the magnetocardiogram, *Journal of Electrocardiology*, 21 (2), pp. 161–167. DOI:10.1016/S0022-0736(88)80012-8.

Tarantola, A. (2005) *Inverse problem theory and methods for model parameter estimation*. Philadelphia, PA: SIAM.

Trayanova, N. A. (2014) Mathematical approaches to understanding and imaging atrial fibrillation: significance for mechanisms and management, *Circulation Research*, 114 (9), pp. 1516–1531. DOI:10.1161/CIRCRESAHA.114.302240.

Tripp, J. H. (1983) Physical concepts and mathematical models, in: Williamson, S. J., Romani, G.-L., Kaufman, L., and Modena, I. (eds.) *Biomagnetism: An Interdisciplinary Approach*. New York: Plenum Press, pp. 101–139.

Uusitalo, M. A. and Ilmoniemi, R. J. (1997) Signal-space projection method for separating MEG or EEG into components, *Medical and Biological Engineering and Computing*, 35 (2), pp. 135–140. DOI:10.1007/BF02534144.

van Dam, P. M., Oostendorp, T. F., Linnenbank, A. C. and van Oosterom, A. (2009) Non-invasive imaging of cardiac activation and recovery, *Annals of Biomedical Engineering*, 37 (9), pp. 1739–1756. DOI:10.1007/s10439-009-9747-5.

van Dam, P. M. and van Oosterom, A. (2005) Volume conductor effects involved in the genesis of the P wave, *EP Europace*, 7 (s2), pp. S30–S38. DOI:10.1016/j.eupc.2005.03.013.

van Leeuwen, P., Hailer, B., Beck, A., Eiling, G. and Grönemeyer, D. (2011) Changes in dipolar structure of cardiac magnetic field maps after ST elevation myocardial infarction, *Annals of Noninvasive Electrocardiology*, 16 (4), pp. 379–387. DOI:10.1111/j.1542-474X.2011.00466.x.

van Leeuwen, P., Hailer, B., Lange, S., Klein, A., Geue, D., Seybold, K., Poplutz, C. and Grönemeyer, D. (2008) Quantification of cardiac magnetic field orientation during ventricular de- and repolarization, *Physics in Medicine and Biology*, 53 (9), pp. 2291–2301. DOI:10.1088/0031-9155/53/9/006.

van Oosterom, A. (1999) The use of the spatial covariance in computing pericardial potentials, *IEEE Transactions on Biomedical Engineering*, 46 (7), pp. 778–787. DOI:10.1109/10.771187.

van Oosterom, A., Oostendorp, T. F., Huiskamp, G. J. and Brake, H. J. ter (1990) The magnetocardiogram as derived from electrocardiographic data., *Circulation Research*, 67 (6), pp. 1503–1509. DOI:10.1161/01.RES.67.6.1503.

Vitikainen, A.-M. (2005) *Sydämen eteisten aktivoitumisreittien määritys magnetokardiografiamittauksista* (Master's thesis). University of Helsinki, Helsinki, Finland. Available from : https://tuhat.helsinki.fi/portal/en/publications/sydamen-eteisten-ak(378e2b5c-1c7e-4b39-af27-14e8babfcf4d).html

Vrba, J., Nenonen, J. and Trahms, L. (2006) Biomagnetism, in: Clarke, J. and Braginski, A. I. (eds.) *The SQUID Handbook*. Wiley-VCH Verlag GmbH & Co. KGaA, pp. 269–389.

Wang, L., Zhang, H., Wong, K. C. L., Liu, H. and Shi, P. (2010) Physiological-model-constrained noninvasive reconstruction of volumetric myocardial transmembrane potentials, *IEEE Transactions on Biomedical Engineering*, 57 (2), pp. 296–315. DOI:10.1109/TBME.2009.2024531.

Wikswo Jr, J. P. (1983) Theoretical aspects of the ECG-MCG relationship, in: Williamson, S. J., Romani, G.-L., Kaufman, L., and Modena, I. (eds.) *Biomagnetism: an interdisciplinary approach*. New York: Plenum Press, pp. 311–326.

Winklmaier, M., Pohle, C., Achenbach, S., Kaltenhäuser, M., Moshage, W. and Daniel, W. G. (2009) P-wave analysis in MCG and ECG after conversion of atrial fibrillation, *Biomedizinische Technik/Biomedical Engineering*, 43 (s1), pp. 250–251. DOI:10.1515/bmte.1998.43.s1.250.

Woods, C. E. and Olgin, J. (2014) Atrial fibrillation therapy now and in the future: drugs, biologicals, and ablation, *Circulation Research*, 114 (9), pp. 1532–1546. DOI:10.1161/CIRCRESAHA.114.302362.

Yamada, S., Tsukada, K., Miyashita, T., Kuga, K. and Yamaguchi, I. (2003) Noninvasive, direct visualization of macro-reentrant circuits by using magnetocardiograms: initiation and persistence of atrial flutter, *Europace*, 5 (4), pp. 343–350. DOI:10.1016/S1099-5129(03)00081-3.

Yoshida, K., Ogata, K., Inaba, T., Nakazawa, Y., Ito, Y., Yamaguchi, I., Kandori, A. and Aonuma, K. (2015) Ability of magnetocardiography to detect regional dominant frequencies of atrial fibrillation, *Journal of Arrhythmia*, 31 (6), pp. 345–351. DOI:10.1016/j.joa.2015.05.003.

Yoshida, K., Tada, H., Ogata, K., Sekiguchi, Y., Inaba, T., Ito, Y., *et al.* (2012) Electrogram organization predicts left atrial reverse remodeling after the restoration of sinus rhythm by catheter ablation in patients with persistent atrial fibrillation, *Heart Rhythm*, 9 (11), pp. 1769–1778. DOI:10.1016/j.hrthm.2012.06.033.

Zar, J. H. (1999) *Biostatistical analysis*. 4th edition. Upper Saddle River, NJ: Prentice-Hall.

Zhou, Z., Jin, Q., Chen, L. Y., Yu, L., Wu, L. and He, B. (2016) Noninvasive imaging of high-frequency drivers and reconstruction of global dominant frequency maps in patients with paroxysmal and persistent atrial fibrillation, *IEEE Transactions on Biomedical Engineering*, 63 (6), pp. 1333–1340. DOI:10.1109/TBME.2016.2553641.

Zimmerman, J. E. and Frederick, N. V. (1971) Miniature ultrasensitive superconducting magnetic gradiometer and its use in cardiography and other applications, *Applied Physics Letters*, 19 (1), pp. 16–19. DOI:10.1063/1.1653725.

Errata for publications

Publication II

The equation on page 176 should read

$$V_m = \sum_{l=1}^{5} \sum_{m=-l}^{l} A_{lm} r^{-l-1} Y_{lm}(\vartheta, \varphi)$$

Aalto-DD 106/2017

ISBN 978-952-60-7466-5 (printed)
ISBN 978-952-60-7465-8 (pdf)
ISSN-L 1799-4934
ISSN 1799-4934 (printed)
ISSN 1799-4942 (pdf)

Aalto University
School of Science
Department of Neuroscience and Biomedical Engineering
www.aalto.fi

BUSINESS +
ECONOMY

ART +
DESIGN +
ARCHITECTURE

SCIENCE +
TECHNOLOGY

CROSSOVER

**DOCTORAL
DISSERTATIONS**